KUOPION YLIOPISTON JULKAISUJA D. LÄÄKETIEDE 357
KUOPIO UNIVERSITY PUBLICATIONS D. MEDICAL SCIENCES 357

MARJA BERG

CT Angiography in the Assessment of Atherosclerotic Carotid and Renal Arteries

Doctoral dissertation

To be presented by permission of the Faculty of Medicine of the University of Kuopio
for public examination in Auditorium, Kuopio University Hospital,
on Friday 10th June 2005, at 12 noon

Department of Clinical Radiology
University of Kuopio and
Kuopio University Hospital

KUOPION YLIOPISTO

KUOPIO 2005

Distributor:
Kuopio University Library
P.O. Box 1627
FIN-70211 KUOPIO
FINLAND
Tel. +358 17 163 430
Fax +358 17 163 410
www.uku.fi/kirjasto/julkaisutoiminta/julkmyyn.html

Series Editors:
Professor Esko Alhava, M.D., Ph.D.
Department of Surgery

Professor Raimo Sulkava, M.D., Ph.D.
Department of Public Health and General Practice

Professor Markku Tammi, M.D., Ph.D.
Department of Anatomy

Author´s address:
Department of Clinical Radiology
Kuopio University Hospital
P.O. Box 1777
FIN-70211 KUOPIO
FINLAND
Tel. +358 17 173 297
Fax +358 17 173 341

Supervisors:
Professor Ritva Vanninen, M.D., Ph.D.
Department of Clinical Radiology
University of Kuopio

Professor Hannu Manninen, M.D., Ph.D., M.Sc.
Department of Clinical Radiology
University of Kuopio

Professor Seppo Soimakallio, M.D., Ph.D.
Department of Clinical Radiology
University of Kuopio

Reviewers:
Docent Pekka Keto, M.D.,Ph.D.
Department of Radiology
University of Helsinki

Docent Tapani Tikkakoski, M.D., Ph.D.
Department of Radiology
University of Oulu

Opponent:
Leena Kivisaari, M.D., Ph.D.
Department of Radiology
University of Helsinki

ISBN 951-781-497-6
ISBN 951-27-0273-8 (PDF)
ISSN 1235-0303

Kopijyvä
Kuopio 2005
Finland

Berg, Marja. CT Angiography in the Assessment of Atherosclerotic Carotid and Renal Arteries.
Kuopio University Publications D. Medical Sciences 356. 2005. 143p.
ISBN 951-781-497-6
ISBN 951-27-0274-6 (PDF)
ISSN 1235-0303

ABSTRACT

BACKGROUND: Atherosclerosis of the artery wall may have serious clinical consequences. The treatment decision often relies on a single measurement of the degree of luminal stenosis detected by imaging. Noninvasive imaging methods have become common as an adjunct or alternative to angiography. The main purpose of this study was to evaluate the feasibility, reproducibility and accuracy of computed tomography angiography (CTA) in the imaging of renal and carotid arteries.

MATERIALS AND METHODS: Renal CTA was performed for 37 patients (Study I) and carotid CTA for 31 patients (Study II) using a single-detector CT device. In study II CTA was compared to three-dimensional (3D) time-of-flight magnetic resonance angiography using digital subtraction angiography (DSA) and intravascular ultrasound (IVUS) as references. Carotid CTA was performed for 36 symptomatic patients using a multidetector CT device (Studies III and IV). For the interpretation of CTA, two-dimensional (2D) and 3D film images (studies I and II), an interactive analysis of 2D images at the workstation (Study IV) and commercial 3D CTA automated analysis software (Study III) were used. The reproducibility of the interpretation of CTA was determined. DSA (Studies I-IV), rotational DSA (Study III-IV) and intravascular ultrasound (Study II) were used as standards of reference.

MAIN RESULTS: CTA proved to be reproducible for the assessment of renal artery stenosis (RAS). Visual analysis of 3D film images was sensitive (100%) in detecting significant ($\geq$ 50%) stenosis in the renal arteries, but specificity was low (42-54%), mainly due to mural calcification at the stenosis site. With different diagnostic algorhythms (i.e. combination of 2D with 3D images or measurement of the degree of stenosis as an adjunct to visual interpretation) the overall accuracy was improved in detecting significant RAS up to 84%, with a slightly lower sensitivity (92%). For the detection of significant RAS, the measurement of renal cortical enhancement provided additional information.

CTA detected minor atherosclerotic lesions in carotid arteries verified with IVUS (Study II). For the measurements of carotid stenosis in symptomatic patients, the results obtained with 3D CTA analysis software were more reproducible than those obtained manually from multiplanar reformations (MPR) by observers using electronic calibers (Studies III-IV). Although the 3D CTA analysis method was automated for the delineation of the contrast-enhanced artery, there were, however, several misregistrations of the boundaries of carotid lumen that required manual corrections. Using rotational DSA as a standard of reference, CTA with MPR measurements overestimated the diameter of the severely stenosed lumen and slightly underestimated the degree of carotid stenosis. Using DSA as a standard of reference, visual analysis was sensitive (100%) in detecting significant ($\geq$ 50%) stenosis in the carotid arteries, with specificity of 73% and overall accuracy of 86%. Using different combinations of image display and diagnostic algorhythms, the specificity and overall accuracy of CTA could be increased (up to 95% and 93%) at the cost of slightly decreased sensitivity (90%). In symptomatic patients, CTA with interactive interpretation was the most accurate method for the detection of significant carotid stenosis, with a sensitivity of 95%, specifity of 93% and overall accuracy of 94%.

CONCLUSION: CTA is reproducible and accurate in detecting atherosclerosis in carotid arteries and significant stenosis in renal and carotid arteries.

National Library of Medicine Classification: WG 500, WG 550, WN 180, WN 206, WL 206, WG 595.C2, WG 595.R3

Medical Subject Headings: arteriosclerosis/diagnosis; diagnostic imaging/methods; angiography /methods; carotid artery diseases/diagnosis; carotid arteries, carotid stenosis; tomography; x-ray computed; comparative study; renal arteries; renal artery stenosis

ACKNOWLEDGEMENTS

This thesis is based on work carried out in the Department of Clinical Radiology, Kuopio University Hospital during years 1994-2005.

I am deeply grateful to my official supervisors, professor Seppo Soimakallio, M.D., Ph.D., and professor Hannu Manninen, M.D., Ph.D., the former and present Head of the Department of Clinical Radiology, for their enthusiastic support throughout this study and for providing all the excellent facilities needed in this work. I owe special thanks to Hannu as my principal supervisor, who originally propelled me into the field of scientific work. His professional suggestions and valuable comments were essential to the outcome of this work. His inspiring working attitude and boundless enthusiasm towards science motivated me during this thesis.

I wish to express my warmest gratitude to my other supervisor, professor Ritva Vanninen, M.D., Ph.D. She patiently taught me the steps of scientific research from designing a study to writing a scientific report. Her wide experience in scientific work with incredibly efficacy is impressive. Her expert guidance was invaluable in completing this thesis. She provided me her tireless encouragement and support throughout this work and also in my personal life as long as we have known each other.

Sincere thanks belong to docent Tapani Tikkakoski, M.D., Ph.D. and docent Pekka Keto, M.D., Ph.D., the official referees of this thesis, who gave valuable criticism and suggestions for completion of the work.

I am grateful to my co-author Zishu Zhang, M.D., Ph.D., who shared the throes of the processing of the two last papers, which was compensated by his amazing stories about life in China.

I wish to express my gratitude to my other co-workers; Pekka Jaakkola, M.D., Ph.D. in the Department of Surgery, and Reetta Kälviäinen, M.D., Ph.D. in the Department of Neurology, to physicists Pauli Vainio, Ph.L. and my colleagues Heikki

Räsänen, M.D., Aki Ikonen, M.D., and Petri Sipola, M.D. Their contribution was essential for this study.

I am grateful to physicists Mervi Könönen M.Sc., and Minna Husso-Saastamoinen, Ph. Lic., for their valuable help in solving problems with computers, statistics and problematic equations.

I am thankful to professor Veli-Matti Kosma, M.D., Ph.D. in the Department of Clinical Pathology, for consultation about histopathology.

I wish to thank Juha Hentunen, M.Sc., for his help with patient data preparation and analysis, and Pirjo Halonen, M.Sc., Information Technology Centre and Kari Mauranen M.Sc., Department of Health Policy and Management, Kuopio University, for their help in statistical problems.

I give my warm thanks to Tuula Bruun, Eija Hassinen and Taina Airola for secretarial assistance. Your valuable assistance laden with humour helped me withstand stressful times.

I also thank the staff of the Kuopio University Library for their help in searching for the literature. I also wish to thank professor Seppo Ylä-Herttuala, M.D., Ph.D., A.I. Virtanen Institute for molecular Sciences and docent Ilkka Tikkanen, M.D., Ph.D., Helsinki University Hospital, for their valuable advice on selecting appropriate articles from the plenitude of the literature for my thesis.

I am thankful to docent David Laaksonen, M.D., Ph.D., MPH, for the linguistic revision of this thesis.

I want to thank all my colleagues in the Department of Clinical Radiology, -you all have somehow shared this work. I thank especially those people who have done all the routine clinical work during those months I was buried in my scientific work. I also thank the radiographers and other personnel of our department.

Special thanks belong to the nurses in the Department of Neurology, who co-ordinated the patients for my last study so well.

I want to thank all my patients who participated in this study.

Finally, I express my dearest thanks to my family and my friends for their support. I express my deepest love to my children Reetta, Erkka, Veikka and Pekka. You are always in my heart.

This work was financially supported by Kuopio University Hospital (EVO funding 5063501), the Radiological Society of Finland, the Pehr Oscar Klingendahl Foundation, the Paavo Ilmari Ahvenainen Foundation, the Maire Taponen Foundation, the Instrumentarium Scientific Foundation and the Finnish Cultural Foundation.

Kuopio, June 2005 Marja Berg

ABBREVIATIONS

CD-US	Colour Doppler Ultrasound
CEMRA	contrast-enhanced magnetic resonance angiography
cMPR	cross-sectional multiplanar reformation
CPR	curved planar reformation
CT	computed tomography
CTA	computed tomography angiography
DSA	digital subtraction angiography
DTPA	technetium-99m-diethylenetiamine penta-acetic acid
ECG	electrocardiogram
ECST	the European Carotid Surgery Trial
HU	Houndsfield unit
ICA	internal carotid artery
IVUS	intravascular ultrasound
MDCT	multidetector row computed tomography
MHz	megahertz
MIP	maximum intensity projection
MPR	multiplanar reformation
MRA	magnetic resonance angiography
MRI	magnetic resonance imaging
NASCET	the North American Symptomatic Carotid Endarterectomy Trial
PACS	picture archiving and communication system
RAS	renal artery stenosis
P	pitch

PTRA	percutaneous renal angioplasty
ROI	region of interest
SDCT	single-detector computed tomography
sMPR	sagittal multiplanar reformation
SSD	shaded surface display
TOF	time-of-flight
US	ultrasound
VR(T)	volume rendering (technique)
2D	two-dimensional
3D	three-dimensional

LIST OF ORIGINAL PUBLICATIONS

The thesis is based on the following original articles, which are referred to in the text by their Roman numerals:

I Berg MH, Manninen HI, Vanninen RL, Vainio PA, Soimakallio S. Assessment of renal artery stenosis with CT angiography: usefulness of multiplanar reformation, quantitative stenosis measurements, and densitometric analysis of renal parenchymal enhancement as adjuncts to MIP film reading. J Comput Assist Tomogr 1998;22(4):533-40.

II Berg MH, Manninen HI, Rasanen HT, Vanninen RL, Jaakkola PA. CT angiography in the assessment of carotid artery atherosclerosis. Acta Radiol 2002;43(2):116-24.

III Zhang Z, Berg MH, Ikonen AE, Vanninen RL, Manninen HI.Carotid artery stenosis: reproducibility of automated 3D CT angiography analysis method. Eur Radiol 2004;14(4):665-72.

IV Berg M, Zhang Z, Ikonen A, Sipola P, Kälviäinen R, Manninen H, Vanninen R. Multidetector CT Angiography in the Assessment of Carotid Artery Disease in Symptomatic Patients: Comparison with Rotational Angiography and DSA. AJNR Am J Neuroradiol 2005;26(5):1022-34.

Unpublished results are also presented in this document.

CONTENTS

1. INTRODUCTION

Atherosclerosis is usually asymptomatic in the early stages of the disease, but advanced atherosclerotic plaques in the artery wall are prone to be symptomatic (1). Obstructing arterial stenosis due to either a large plaque or sudden intraplaque haemorrhage of a plaque and plaque rupture with thrombosis are the main causes of symptomatic disease. Symptoms are related to the endorgan supplied by the diseased artery. Atherosclerosis plaques in the carotid and coronary arteries may cause life-threatening or strongly disabling disorders. Although the cornerstones of the treatment of atherosclerosis are appropriate medication and changes in life-style, i.e. cessation of cigarette smoking and making alterations in diet and exercise habits, the treatment of atherosclerotic manifestations also includes surgical and endovascular interventions.

Before the choice of the treatment, the extent of the atherosclerotic disease and the need for interventions are verified by imaging. Catheter angiography has been the most common imaging method, but non-invasive imaging methods such as grey scale ultrasound with a B-mode, colour-Doppler ultrasound (CD-US), magnetic resonance angiography (MRA) and CT angiography have partly replaced invasive angiography. Despite some disadvantages of CT angiography imaging, such as radiation and use of potentially nephrotoxic contrast media, CT angiography is feasible for the imaging of atherosclerotic arteries when the patient selection and preparation before the scanning are well done. Over the last decade, the development of CT devices has widened the scope of this nowadays rapid and easy imaging method to include the arteries. Furthermore, CT angiography is more convenient and less time consuming for the patient than catheter angiography.

However, proper verification of the reproducibility and accuracy of CT angiography will define the actual indications in which CT angiography should be used in clinical practise.

2. REVIEW OF THE LITERATURE

2.1. ATHEROSCLEROSIS

2.1.1. Risk factors

Risk factors including age, smoking, total cholesterol and systolic blood pressure or hypertension were strong predictors of the progression of mild to severe extracoronary atherosclerosis in the elderly in a a population-based cohort study (Rotterdam study) (2). Diabetes mellitus predicted progression of severe atherosclerosis (2). The association of high-density lipoprotein cholesterol and coronary disease has proved to be inversed (3). In addition, several psychological factors, including depression and chronic life stress, may have direct pathophysiological consequences with respect to the exacerbation of coronary artery disease.

A very high stroke attack incidence for men has been detected in the Kuopio area in Finland, higher only in Novosibirsk, Russia. This incidence detected in WHO MONICA study in 2002 is three times higher than in Friuli in Italy (4). That may indicate the prevalence of some detrimental genes increasing atherosclerosis in the Finnish population. However, the impact of genes on the risk of atherosclerosis does not dominate over the impact of environmental factors (5). It should be noted that many of the biomechanical and physiological factors exist throughout the lifespan, not only in the elderly who suffer the manifestations of atherosclerosis. Insulin resistance phenomenon potentially leading to the metabolic syndrome is one example of a clinical abnormality that appears already during childhood, and leads to clustering of risk factors for some individuals (6). Endothelial dysfunction is supposed to be linked to the risk of atherosclerosis in diabetic children (7).

Several attempts have been made to reduce risk factors in the population in the primary and secondary prevention of atherosclerosis and related diseases. Although many of these risk factors potentially could be reduced with lifestyle changes or medical treatment of blood pressure or high total cholesterol in patients with coronary artery disease, a common problem in several geographical areas including Finland is the lack of effectiveness in achieving these preventive goals, as shown in the EUROASPIRE study (8). However, the North Karelia Project, a cardiovascular health programme in Finland, has succeeded in decreasing the general risk factor level of the population (9). In addition, lifestyle interventions such as exercise, healthy food and weight control can reduce the incidence of type 2 diabetes, a risk factor for the progression of atherosclerosis, among individuals with overweight (10).

2.1.2. Pathophysiology and morphology of the atherosclerotic plaque

In recent investigations three main elements are considered to be important in the genesis of atherosclerosis; cholesterol, infection and inflammation. The relative importance of these factors is still unknown (11). However, in autopsies of children killed in accidents the clustering of modified cholesterol without inflammation in artery wall has been noted. In addition, several viruses have been proposed to be related to the generation of atherosclerosis (11).

The transport of cholesterol inside the artery wall is dependent on the concentration in the blood. The intima layer is different from other tissues in that the intima lacks the lymphatic drainage, which actively transports cholesterol from the extracellular space. Various molecules, enzymes and matrix produced by cells in the intima are crucial for the modification of the atherosclerotic process in the intima layer (12). Especially modified lipoproteins generate a vicious circle.

In the walls of arteries, fatty streaks containing lipid-rich macrophages and smooth muscle cells and intimal thickening have been proposed to be precursors of atherosclerosis (13). Development of fatty streak includes transport, retention and modification (oxidation) of lipoprotein inducing monocyte migration, differentiation and foam cell formation (14). Smooth muscle cells in plaques differ from those in the media layer, although it has been suggested that they have migrated from the media layer to intima. The extracellular matrix of fibrous plaques is produced by smooth muscle cells (14). The advanced atheromatous plaques have a lipid core consisting mainly of free cholesterol and cholesterol esters. Apoptosis of macrophages and smooth muscle cells precedes the formation of vulnerable plaque. The lipid core is covered by fibrous tissue called as fibrous cap. A thin fibrous cap is prone to rupture, especially in the 'shoulder' area, leading to haemorrhage and thrombosis. The degradation of the structural proteins of the plaque, mainly collagen, might be mediated by interstitial collagenase (matrix metalloproteinase-1) producted by cells in the plaque (15). Also formation of neovasculature and sometimes intraplaque haemorrhage are seen in atheromatous plaques.

Calcium deposits and even bone formation are common in atherosclerotic lesions (16). Calcium deposits may involve the mechanical properties of the atherosclerotic plaque (14), but the patients with large calcium deposits are thought to have less clinical events (16, 17).

Recently, two alternative hypotheses have been propoused to explain the accumulation of lipoproteins in the artery wall (18, 19). Kologie et al (18) have proposed on the basis of their experimental study that accumulation of free cholesterol is related to intraplaque haemorrhagic events and cholesterol of the plaque originates from the cholesterol-rich erythrocyte membranes. Another

hypothesis suggests that mast cells actively accumulate cholesterol as dropplets precipitating the formation of foam cells (19).

Atherosclerosis has certain sites of predilection, for example at the bifurcation of the carotid arteries, which are exposed to haemodynamic stress and further to inflammation. There are lesions of different phases in different parts of the arterial system. Atherosclerosis is a dynamic process, and not inevitable (12).

2.1.3. Clinical manifestations

Cardiovascular diseases are the leading cause of mortality in Finland (Statistics Finland; www.stat.fi/index_en.html). The clinical manifestations of atherosclerosis as a systemic disease depend on the end organ supplied by the diseased artery. In addition to carotid arteries and renal arteries discussed more thoroughly later, atherosclerosis of coronary arteries, lower limb arteries and visceral arteries are the most important vascular areas causing morbidity and mortality. The leading cause of morbidity is ischaemic coronary disease. Cerebrovascular disease with disabling stroke is still the leading cause of long-lasting morbidity.

2.1.3.1. Renal artery atherosclerosis

The morphology of the atheromatous lesions in renal artery is similar to those in other vascular sites (20). Aortic wall atherosclerosis can also involve the origin of the renal artery causing ostial stenosis (21). The atherosclerotic lesion in renal artery may locate in any part of the vessel and also in accessory renal artery, although the atherosclerotic lesion locates more frequently in the main renal artery near its origin.

The importance of atherosclerotic occlusive lesions in renal arteries is associated with renovascular hypertension and renal failure (22). It has been estimated that

renovascular hypertension is the aetiology of hypertension in 5% of cases (20). Any flow restriction, caused by atherosclerosis in 60% of cases, or in the remaining cases by other factors such as fibromuscular disease, may cause renovascular hypertension. Renovascular hypertension has a well-known pathophysiology mediated via the renin-angiotensin system (23). However, not all patients with atherosclerotic occlusive lesion have renovascular hypertension.

Atherosclerotic lesions in the aortic wall or in renal artery are possible sources of atheromatous or cholesterol emboli. Especially during intervention the plaque is predisposed to rupture. Renal ischaemia due to flow restriction or emboli induces renal infarction, which in the worst cases leads to loss of the whole kidney (20).

2.1.3.2. Carotid artery atherosclerosis

The prevalence of severe stenosis due to carotid atherosclerosis is not common in the unselected population, and often carotid atherosclerosis is asymptomatic (24). The aortic arch, carotid bifurcation, carotid siphon, distal vertebral arteries and basilar artery are the predilection sites of atherosclerosis in the Caucasian population (24). In early atherosclerosis fatty streaks involve carotid arteries later than the aortic wall. Atherosclerosis in the artery wall supplying the brain is a risk factor for stroke and other cerebrovascular disorders, i.e. amaurosis fugax, transient ischaemic attacks and dizziness. Stenosis, wall thickness, the lipid or necrotic core of the plaque, plaque ulceration and intraplaque haemorrhage are supposed to be related to the risk of stroke and other cerebrovascular disorders, but the data concerning the relationship between plaque morphology and clinical outcome are still conflicting (24-26). However, both haemodynamic and embolic mechanism are supposed to produce disorders (24).

The degree of stenosis has been reliably verified to be related with stroke risk. When the large randomised multicentre trials, European Carotid Surgery Trial (ECST) in 1981 and the North American Symptomatic Carotid Endarterectomy Trial (NASCET) in 1987, were launched to compare the risk of stroke between medically and surgically treated patients, conventional angiography was the main imaging method to detect of carotid stenosis. Those trials have shown that carotid endarterectomy is beneficial in the secondary prevention of stroke in symptomatic patients with high-grade stenosis (27-29). In the NASCET study, the cumulative risk for ipsilateral stroke were 26% in the medical patients and 9% in surgical patients (27). In the pooled data from these randomised controlled trials, some benefit was noted in patients with a 50-69% stenosis, whereas the benefit in patients with carotid a near occlusion has been reported to be marginal in the short-term and uncertain in the long-term (30). Furthermore, the benefit of carotid endarterectomy in various subgroups of disorders and angiography findings must be considered in treatment decision making (31).

In addition, randomised studies for asymptomatic carotid stenoses have verified decrease of the risk for stroke in patients with carotid stenosis greater than 60%, but only with perioperative risk of 3% or less (32, 33). An ongoing randomised study includes the plaque characterisation for the observation of subgroups at stroke risk (34).

2.1.4. Treatment of atherosclerotic manifestations

2.1.4.1. Renal artery stenosis

In general, the first choice of treatment for treatment of hypertension is lifestyle changes and medication. Resistant hypertension to several pharmaceuticals,

generalised atherosclerosis or progressive renal failure, especially in conjuction with angiotensin-converting enzyme inhibitors, often arouse suspicion of a renovascular mechanism causing hypertension (22).

In most patients hypertension is either cured or improved with surgery of the stenosed unilateral or bilateral renal artery (35). Surgical treatment includes a wide variety of techniques (36). Anatomic and extra-anatomic reconstructions can be performed to by-pass the stenosed renal artery, and autogenous tissue has been considered to be preferable for reconstructions rather than the use of prosthesis (36). Patients with renovascular disease due to atherosclerosis are challenging, because they often also have impairment of renal function and generalised atherosclerosis exposing to embolic and cardiac complications during operation. Advanced age and clinical congestive heart failure have shown to be the predictors of perioperative death (35).

Since the establishment of interventional radiology, i.e. endovascular therapy, the number of operations for the treatment of renovascular disease has declined in many centres. Endovascular intervention is preferable for patients at risk for perioperative complications. The transfemoral approach is often used for renal artery interventions, but brachial artery access is an alternative pathway for the intervention (37). Percutaneous transluminal renal angioplasty (PTRA) has proved to be as effective as surgery in the short-term with lower costs, lower complication rates and shorter patient recovery times. The long-term results of PTRA also have proven to be favourable, but in some cases conversion to operative treatment or reintervention is needed (38). PTRA with stenting has a better outcome in ostial atherosclerotic stenoses than PTRA alone (39). PTRA with stenting can also be used as a rescue

therapy in restenosis after PTRA. Furthermore, renal failure has also been included as an indication for PTRA with stenting (40).

2.1.4.2. Carotid artery atherosclerosis

Carotid endarterectomy of a haemodynamically significant stenosis in patients with symptoms, but not with a severe neurological deficit, reduces the risk for stroke. Otherwise antiplatelet or anticoagulant therapy should be preferred (41). In carotid endarterectomy with or without shunting, the atheromatous plaque is dissected via arteriotomy from the artery wall of common carotid, external carotid and internal carotid arteries (41). During operation, the patient should be given systemic heparin and careful monitoring of blood pressure and electroencephalogram (ECG) should be performed. Postoperative follow-up of blood pressure is also mandatory to avoid haemorrhagic complications. Data from large clinical randomised trials such as NASCET and ECST are helpful for making treatment decisions in different subgroups of patients (42).

Based on the reports of published studies, the role of endovascular treatment of carotid stenosis still is developing. In the randomised CAVATAS trial (43), angioplasty of carotid stenosis with or without stenting had similar effectiveness and a similar rate of major complications as carotid endarterectomy. The CAVATAS trial has been criticised for having too many complications in both the endovascular arm and in the surgical arm (44), but it should be noted that majority of the patients of the CAVATAS study underwent only angioplasty without stent placement. Currently the stent placement is done invariably. One early randomised study comparing the effectiveness of carotid angioplasty versus carotid endarterectomy was stopped due to a high complication rate in the nonprotected stenting group (45). However,

endovascular treatment should be considered for patients excluded from surgical treatment due to high perioperative risks, and stenting of carotid stenosis reduces the rate of reinterventions due to restenosis (46).

A major periprocedural complication in CAVATAS trial was stroke, which may be caused by embolic material from rupturing atherosclerotic plaque. In a cadaver study, no difference was found in distal embolisation between angioplasty alone and stenting (47). The use of a protection device may reduce embolic complications of endovascular treatment (48, 49). The investigators of CARESS study suggest that the 30-day risk of stroke or death following carotid stenting with cerebral protection is equivalent to carotid endarterectomy (50). In a large prospective study carotid artery stenting with or without cerebral protection device, the procedure was successful in 98% of cases (3207/3267) with a combined morbidity and mortality rate of 2.8%, but the authors have not yet reported the results separately according the use of the cerebral protection device (51). The investigators of the SAPPHIRE trial suggest that carotid stenting with a protector device is a reasonable alternative to carotid endarterectomy in patients at high risk of perioperative complications (52). Several randomised trials for the evaluation of the effectiveness of carotid stenting incorporating cerebral protection versus carotid endarterctomy have been started (53-56). The Technology Assessment Committees of the American Society of Interventional and Therapeutic Neuroradiology and the Society of Interventional Radiology have recently published reporting standards for carotid artery angioplasty and stent placement (57).

2.2. IMAGING OF ATHEROSCLEROSIS

2.2.1. CT angiography

2.2.1.1. Development of CT angiography

Since the advent of CT equipment for clinical imaging, the development of spiral (or helical) CT with a slip ring scanner was the main step towards the evolution of CT angiography. Continuous CT spiral scanning with breath-holding of the patient and simultaneous patient transport through the gantry allowed volumetric imaging of whole organs without discontinuities (58, 59). This rapid spiral volumetric CT scanning permitted imaging of the organs optimally in the arterial or venous phase during the first pass of an intravenously injected bolus of contrast media. Soon after spiral CT scanning was introduced in 1990, several of the first reports on the clinical applications of spiral CT concentrated on CT angiography (60-63). Rapid volumetric scanning increased image noise slightly and induced a minor decrease in the z-axis resolution, but did not decrease the diagnostic quality of the study (64). Methods for three-dimensional (3D) display were generated before the introduction of CT angiography. The 3D display with 'angiographic-like' images was quickly adopted for demonstration of CT angiography studies (61, 65-67). With overlapping axial source images the z-axis resolution was improved, upgrading also the quality of reconstructed images (68).

In the first series the scanning volume in single-detector CT (SDCT) angiography was relatively short, depending on the imaging parameters such as collimation and table feed. The introduction of 180° linear and higher-order interpolation algorithms showed that table feed could be increased over the length of slice collimation (pitch values over 1), with a slight increase in image noise, but longer scanning volumes (69, 70). Because individual circulation time sometimes led to suboptimal arterial

contrast enhancement, a method for the detection of optimal scan delay time was developed, replacing the use of fixed delay time (70). Later manufacturers produced special programs for automatic detection of contrast material arrival into target vessels, i.e. bolus triggering methods. Within five years, CT angiography has been used to image almost all arteries from head to toe (66, 71, 72), and also venous structures (73, 74).

In the early days of CT angiography the total examination time, including the time for scanning, postprocessing of the images and the image display, was up to 1.5 hours. Gradually, the overall duration of CT angiography has decreased. The capacity and heat-resistance of x-ray tubes increased, also allowing longer scan times. Furthermore, data acquisition time has decreased with subsecond scanning, which also improves the imaging of small arteries (75). Computers have become more powerful, resulting in faster reconstruction of raw data. With effective computers the real time interactive volume rendering (VR) method for 3D display has become available for clinical use (76). Finally, advanced CT equipment with multiple-row detectors (MDCT) opened a new era for CT angiography, eliminating many disadvantages such as large doses of contrast media, some artefacts and limited scan volume coverage (77, 78). Nowadays, this 'multislice' CT angiography with rapid interactive modes for image display has achieved a firm standing in the repertoire of noninvasive methods for vascular imaging.

2.2.1.2. Technique of CT angiography

2.2.1.2.1. Preparing of the patient for CT angiography

Preparing the patient for CT angiography is simple. To perform CT angiography, it is mandatory that the patient can co-operate. Before the study all phases of the

examination should be explained to the patient to obtain good quality images without movement artefacts. A history of previous hypersensibility reactions of the patient should be asked, especially if caused by iodinated contrast agents. For abdominal studies, water or fat-based oral contrast material can be used, if needed. Iodine- or barium-based oral contrast agents are not desirable. Because the contrast media may be nephrotoxic, before CT angiography renal function should be evaluated to avoid use of contrast media for patients at risk for contrast-induced renal failure (79). The screening of renal function with laboratory tests, most often serum creatinine, from patients without risk factors has been questioned based on a study with 2034 outpatients, because renal function impairment is very seldom amoung patients without known risk factors (80). Recently, the European Society of Urogenital Radiology has produced a simple guideline on serum creatinine measurements before iodinated contrast medium administration (79). If needed, sufficient hydration for the patient should be arranged. For the contrast media infusion, an 18-gauge cannula is placed in the antecubital vein. Unenhanced images from the target area for localising anatomical structures are obtained, if necessary.

2.2.1.2.2. SDCT angiography

The planning of CT angiography examination using a single slice device must be done with caution due to the limited coverage of imaging volume obtained with the SDCT device. The scanning time also extends up to 30-40 seconds with the larger imaging volumes, for example in imaging of aorta, which may exceed the breath-holding capability of the patient.

In general, a thin collimation should be chosen to optimise longitudinal (Z-axis) resolution. A slow table feed and a small reconstruction interval are preferable to

image small vessels, especially those running in the axial plane (81). Naturally, minimising those parameters will decrease the length of the scanning volume. To meet the need for good resolution and sufficient scan volume, it is preferable to increase the pitch (=table increment per gantry rotation/collimation) rather than to increase the size of collimation. The section sensitivity profile impairment using thinner collimation with a faster table feed, allowing longer scan, is only moderate compared to the use of collimation size equal to the table feed length per second. Then the pitch (P) value increases to over 1, but it should not exceed the value of 2 (69). The noise is related to other imaging parameters such as collimation and x-ray tube output (kilovoltage, tube current), but not to the pitch value (82). Most clinical applications of CT angiography can be performed with 3-5 mm collimation using an SDCT device, but for small size vessels, a thin collimation of 1-2 mm is preferable. The reconstruction increment and section widht for axial source images should be chosen so that axial slices overlap at least 50%. Detailed protocols for SDCT angiography of specific anatomic regions have been published (83-85).

2.2.1.2.3. MDCT angiography

The first dual-slice scanner was originally developed in 1991, but advanced MDCT devices with two different detector array designs (matrix detectors and adaptive array detectors) were introduced in 1998. These devices allow larger anatomic coverage, for example imaging of the entire aortoilac system and lower extremity inflow and run-off (78, 86). At present, MDCT devices are available with up to 64 rows of detectors with subsecond rotation. This technology allows faster scanning, excellent spatial resolution with isotropic imaging, multiphase studies and convenience for the patient because the breath-holding time is shortened. Also new applications, i.e.

cardiac and coronary artery imaging, have been introduced. All these advancements can contribute to the increase of diagnostic utility.

The speed of subsecond scanning with multiple detectors allows the routine use of thin collimation, ensuring high spatial resolution and good quality reformations. The latter also warrants at least 50% overlapping of axial source images. One of the advantages of MDCT imaging is flexibility. For most multidetector row CT equipments, spiral raw data can retrospectively be reconstructed at different slice thickness values and increment values, but the section widht (slice thcikness) should not be less than the thickness of the collimation. Also with MDCT the table speed and the rotation time of the scanner influence the scanning volume coverage. The limited scan coverage of four detector row MDCT devices is evident with a high-resolution protocol (87).

There are two definitions for the pitch value of MDCT. In practise most vendors use the definition P*=Table feed (mm) per gantry rotation/slice collimation (mm), where the value is dependent of the number of detectors, while slice collimation is for a single active detector (87). Some authors have recommended using the original equation, where pitch is defined as in SDCT: P=Table feed (mm) per gantry rotation/beam collimation (mm). These two definitions of pitch are related to each other P*= n x P, where n is the number of active detector channels and these definitions are called as 'volume pitch' (P*) and 'detector pitch' (P) (88). Different protocols are available for each anatomic region with respect to the indication for vascular imaging and for different multislice devices (78, 87, 89-94). For patients with overweight it is possible to change imaging parameters and the interpolation algorithm to improve the quality of images (86).

2.2.1.2.4. Contrast media application

It is desirable to perform the contrast media injection with a double-syringe power injector for the contrast media injection and subsequent saline flush. The saline flush pushes the contrast media to central circulatory and flushes the veins free from high concentration of contrast media related to strike artefacts. Artefacts from contrast-filled veins also can be avoided by changing the scanning direction (i.e. from craniocaudal to caudocranial for the imaging of carotid arteries).

The circulation time of the patient should be determined if there is doubt about decreased cardiac output increasing the time between the start of the contrast media infusion and the arrival of contrast media in the target vessel. The determination of circulation time can be carried out with a test bolus or with specific programs, i.e. bolus triggering methods, which are nowadays widely available in CT devices (85, 95). These bolus triggering methods monitor the inflow of contrast media to the target vessel with continuous low-dose scanning.

Enhancement in the target vessels is affected by patient-related and injection-related factors. Body weight is the most important patient-related factor; an increase in body weight decreases the arterial enhancement (96). Low cardiac output delays the peak enhancement, but increases the enhancement magnitude. In vascular imaging, the enhancement is directly related to the iodine concentration in target vessels (96, 97). A high concentration in target vessels can be reached with an increase in flow rate of commonly used contrast media (300 mgI/ml) or with the use of high-concentration contrast media (370 or 400 mgI/ml). Additional benefit can be achieved with the use of high-concentration contrast media with early enhancement (97).

Because the resolution to noise relationship is proportionally affected by the contrast media concentration in target vessel, the contrast media infusion should be planned carefully. The duration of the scanning is critical for the planning of contrast media application. Using SDCT the scanning duration time is almost always long, up to 40 seconds. Some special MDCT imaging protocols with a long scanning time for example ECG-gated cardiac imaging, require extended contrast media infusion. With the use of extended contrast media infusion, the total amount of iodine given to the patient should be controlled.

A basic understanding of the contrast media kinetics after intravenous bolus infusion is essential to perform CT angiography studies (98). In general, the iodine administration rate has to be increased for angiography examinations with MDCT to obtain satisfactory enhancement in the target vessels. The iodine administration rate could be increased using a higher flow rate of the infusion or alternatively using high-concentration contrast media. However, due to faster scanning of MDCT the total volume of contrast media infusion is substantially lower than using SDCT for CT angiography. The critical point for contrast media infusion for MDCT angiography examinations is the very short time window for the data acquisition, because in most general applications for vascular imaging the scanning lasts only 5-10 seconds (98). The exact time delay from the beginning of the intravenous infusion to the arrival of the contrast media in the target vessel is crucial due to the short data acquisition time, because if timing fails, the enhancement in target vessels could be totally missed. Therefore, the use of bolus triggering technique is essential for the MDCT angiography studies. Specific contrast infusion protocols for different duration of data acquisitions are published and it is also recommended to use biphasic protocols to achieve uniform enhancement in CT angiography (98, 99).

In addition, a noteworthy point for the improvement of the CT angiography quality is appropriate scanning technique, because low kVp enhances the attenuation of radiation in vascular studies increasing the ratio of resolution to noise and visualisation of vascular structures (100). Furthermore, with the use of low kVp the dose of radiation decreases concurrently.

2.2.1.2.5. Reformations and 3D-reconstructions of CT angiography

The axial data of CT angiography can be demonstrated with reformations (two-dimensional display) or with three-dimensional (3D) reconstructions. The reformation techniques, multiplanar reformation (MPR) and curved planar reformation (CPR), retain the original image data of axial source images including high attenuation structures such as enhanced vessels and mural calcifications and low attenuation structures such as intimal plaques and trombi. Two-dimensional MPR is a widely used postprocessing technique and with arbitrary chosen views, it is very useful in CT angiography (101-103). Thin MPR with good resolution for vessel display shows usually only restricted views of the tortuous vessels demanding a serial of MPRs over the region of interest. With CPR it is possible to follow the entire course of the vessel (Figure 1). In general, CPR is not suitable for measurement of diameters due to the distortion of structures. However, there is commercially available software with automatic assessment of the vessel using CPR, where the automatic assessment of the center of the lumen facilitates accurate measurements of vessel cross-sectional dimensions.

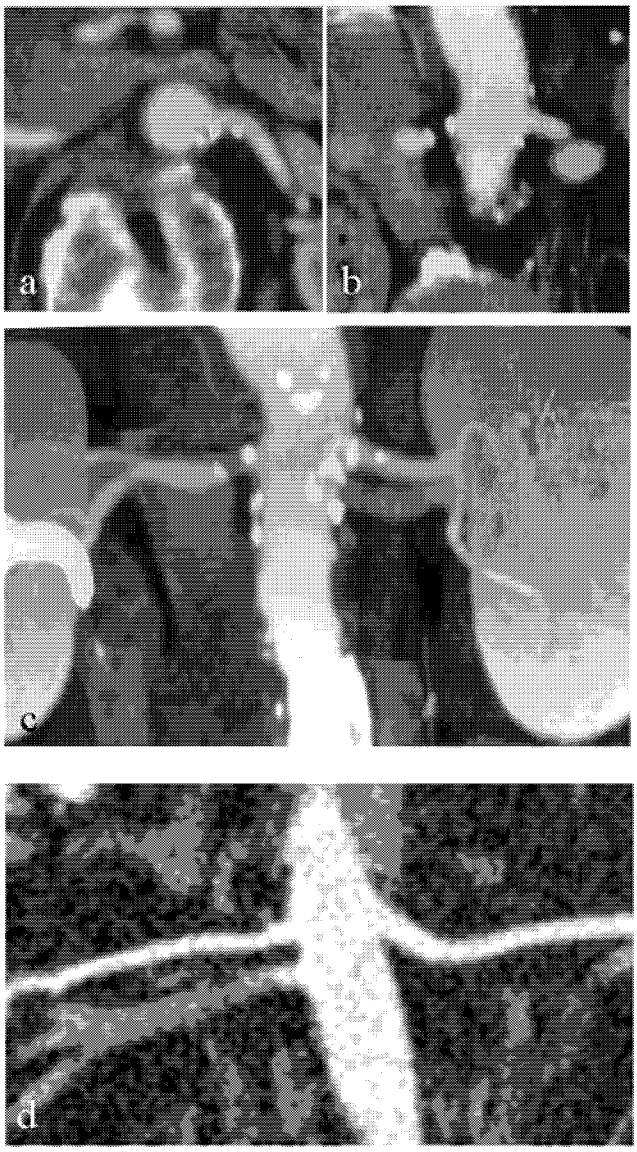

Figure 1.

CT angiography images of two different patients. One original axial image (a) and single coronal multiplanar reformation image (b) of renal arteries shows only limited view. Maximum intensity projection (c) and curved multiplanar image (d) demonstrates the main renal arteries.

For the 3D display using maximum intensity projection (MIP) or shaded surface display (SSD) the editing of unnecessary structures, such as bones and enhancing veins and organs, is essential (102). MIP retains the voxel with the maximum intensity in each line, in CT angiography mainly the voxels containing enhanced vascular structures (104). MIP misses the visualisation of depth, leading sometimes to misinterpretation of the anatomical relationships. In MIPs, differences in attenuation can be detected, thus plaque mural calcifications are distinguishable but especially an extensive mural calcification hampers the demonstration of vessel lumen. Intraluminal pathology may be obscured if it is surrounded by enhanced blood flow; hence the detection of intravascular trombi, emboli or dissection is limited in MIP (104). Sliding thin-slab MIPs are also useful for the demonstration of the complex vascular structures (105). Targeted MIP is useful to avoid artefacts from overlying structures.

For SSD images, one or two user-defined thresholds are chosen, and only those high attenuation voxels inside chosen two thresholds or over one chosen threshold are displayed (106). The impression of depth is computed with a virtual light source. SSD images in CT angiography are feasible for visualising complex vascular anatomy, but this method suffers from the inability to show structures separately, i.e. in CT angiography this method fuses vascular structures and plaque calcifications (65).

With the aid of powerful computers the volume rendering (VR) technique has developed into one of the most fascinating technique for 3D image display. The primary principle of the VR technique is to maintain the original data of CT examination without cumbersome and obsolete editing of the axial data. VR technique uses data from all imaged voxels through volume data management. VR

image formation for display consists of algorithms for transfer functions (107). Maintainance of the data from all voxels in VR allows the editing of 3D display with a clip plane in real time. VR technique can also be used for the purpose of virtual endoscopy in addition to the SSD technique (108).

2.2.1.2.6. Interpretation of CT angiography

For the purpose of CT angiography image display several methods are available as described above. However, the radiologist must be aware of the technical principles underlying those 3D reconstruction methods to avoid pitfalls in the evaluation of vascular lesions (101, 102, 109). The editing of axial slices must be done with caution to avoid removal of valid data. MIP lacks impression of depth, leading to overprojection of structures. While only those voxels containing the highest intensity are displayed, other valid data of the same ray with lower attenuation might be obscured. The selection of threshold is of greater significance for SSD. Incorrect threshold selection can falsely imply or exclude lesions, i.e. stenosis, in arteries. Although the VR technique for 3D image display consists more of the original data than MIP or SSD, all the pathology detected in VR must be confirmed from the source images. This also applies to other 3D display techniques (101).

Instead of immediate use of the 3D display methods, it is preferable first to interpret a CT angiography study using original data without data editing or conversion (104). Axial source images and MPR contain all the information of the entire imaged volume, such as enhanced vascular structures, plaques in the arterial wall with or without mural calcifications and extravascular tissues. The quality of MPR images has improved since the advent of MDCT, which allows the routine use of thin collimation, leading to high spatial resolution and nearly isotropic or isotropic voxel

size (87). In addition, MPR images are easy to reconstruct without time-consuming editing of source images or removal of mural calcifications. MPR does not suffer from the overprojection of the other enhanced vessels. However, a single axial image or MPR view displays only a substructure of an arterial tree. The interpretation of the complex vascular system necessitates viewing of several contiguous axial images or MPRs. Therefore the interpretation has to be done on a workstation using a cine mode. This is called interactive interpretation (109). The interactive interpretation of CT angiography in our daily practice includes scrolling of axial source images together with two MPR views in orthogonal directions (sagittal and coronal) to analyse vascular anatomy and pathology. If necessary, additional MPR views angled by the direction of the viewed vessel or curved reformats are done. CT angiography with this interactive volumetric interpretation is an advisable and beneficial tool for the radiologist to analyse vascular anatomy and pathology. The 3D display methods are an additional tool for the overview of the anatomy, for the search of possible sites of pathology, and for the demonstration of the diagnosis to the referring physician (101). In addition, the 3D images can display complex arterial anatomy in a single view, as shown in Figure 2 displaying 3D reconstruction images of the epiaortic and entire carotid circulation imaged with a 16-row multidetector device.

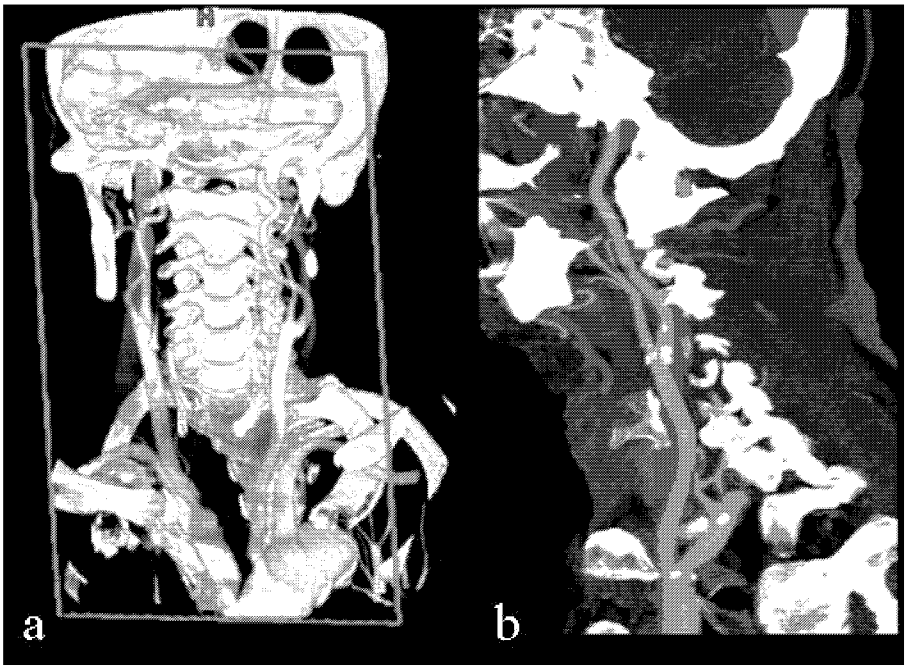

Figure 2.
Carotid artery anatomy of two different patients shown with 3D reconstructions. VR image (a) shows the entire course of both carotid arteries. Thin slab MIP (b) shows the entire course of the extracranial right carotid artery with mural calcifications at the bifurcation.

2.2.1.3. CT angiography of renal arteries

Early in the advent of CT angiography the aorta and its branches, including the renal arteries were incorporated to the repertoire of the vessels imaged with this minimally invasive method (65). A review of designs and results of studies comparing the diagnostic performance of SDCT angiography with conventional angiography as a standard of reference for the diagnosis of renal artery stenosis is shown in Tables 1 and 2.

Table 1. The design of SDCT angiography studies on renal arteries

Study	Contrast media				Imaging parameters			
	Volume ml	Consentration mg I/ml	Flow rate ml/s	Test bolus or bolus triggering +;yes, -;no*	Collimation/Slice thickness (mm) †	Feed/pitch	Increment (algorithm in parenthesis)	Tube Current
Galanski, 1993 (63)	100 – 150	300	3,5 (3-5)	+	2 (2 – 3)/2	2-3/1	1 – 2	NA
Rubin, 1994 (70)	90 – 150	300	3 (90 ml) 5 (150 ml)	- for 8 patients (20 s) + for 23 patients	3/NA	3/1 or 5 – 6/1.67 – 2.0	2	120 KV 165 – 210 mA
Olbricht, 1995 (110)	100 – 150	300	3 – 5	+	2 (2 – 3)/2	2-3/1	1 – 2	NA
Van Hoe, 1996 (111)	100 – 150	380	3,5 – 4/ 1,5 – 3	+	2/NA	2/1	1 (180 ° LI)	120 kV 165 mA
Beregi, 1996 (112)	120	300	4	+	3/NA	3/1	1 (360° LI)	137 kV
Kaatee, 1997 (113)	140	300	3	- for 35 patients (27 s) + for 36 patients	3/NA	3/1	1 (180 ° LI)	140 kV 250 mA
Kim, 1998 (114)	100 – 150	370	2.8 – 3.5	- (18 – 22 s)	3/NA	3-6/1 – 2	1 (180 ° LI)	NA
Johnson, 1999 (115)	120	300	4	+	1/NA 3/NA	NA/2 NA/ 1 – 2	1 for 1 mm collimation 1.5 for 3 mm collimation	120 kV 260 – 280 mA
Wittenberg, 1999 (116)	100 – 150	300	3	+	2/NA	2/1 3/1,5	1 (360 ° LI / 180 ° LI)	120 kV 165 mA
Wilhelm K, 2000 (117)	125	NA	3	- (25 s)	NA/2	3/NA	1 (180 ° LI)	NA

Note – NA, not available; LI, linear interpolation

*The fixed delay time in parenthesis

† If NA, probably slice thickness is the same as the width of collimation

Table 2. Diagnostic performance of renal SDCT angiography in comparison to conventional angiography: A review of the literature

Study	n vessels (patients)	The criteria for the significant finding	Method for interpretation	Results				
				Image display	Sensitivity %	Specificity %	Overall accuracy %	Other
Galanski, 1993 (63)	54 (22)	Five point scaling	Visual interactive	Axial+MPR+MIP+SSD	NA	NA	NA	4/22 false positives or negatives
Rubin, 1994 (70)	33 (31)	≥ 70% (grade 2-3)	Visual	MIP SSD	92 59	83 82	80 55	
Olbricht, 1995 (110)	157 (62)	≥ 50%	Visual interactive	MPR+MIP+SSD	98	94	NA	
Van Hoe, 1996 (111)	20 (14)	Grade 0< 50% Grade 1 = 50-69% Grade 2 = 70-99%	Visual interactive (MIP 1 and 3) or hard copies (MIP2)	 MIP 1 MIP 2 MIP 3 Two-step*	NA	NA	Grade 1 / Grade 2 75 – 85 / 82 – 85 85 – 85 / 75 – 75 75 – 85 / 80 – 85 100 – 100 / 95 – 100	
Beregi, 1996 (112)	131 (50)	≥ 50%	Visual interactive	Axial+SSD+MIP+MPR	88 100†	98 98 †	NA	
Kaatee, 1997 (113)	166 (71)	Grade 0=0 Grade 1=1-49% Grade 2=50-99% Grade4=100%	Visual	Axial+MPR+MIP	Grade 1 97 Grade 2 92 Grade 3 96 Grade 4 100	100 98 96 100	NA	
Kim, 1998 (114)	127(50)	≥ 50% ≥ 75%	Visual	MIP (axial)	90 88	97 99	NA	
Johnson, 1999 (115)	61 (25)	≥ 50%	Visual interactive	MIP VR	94 89	87 99	89 97	
Wittenberg, 1999 (116)	197 (82)	> 50%	Visual interactive	Axial+SSD+MIP+MPR for calcified stenoses	85.8	99.4	98.9	
Wilhelm, 2000 (117)	76 (38)	> 50%	Visual	Axial MPR MIP Axial+MPR Axial+MIP	84 76 76 96 92	96 81 70 100 96		

Note – NA, not available; MPR, multiplanar reformation; MIP, maximum intensity projection; SSD, shaded surface display; VR, Volume rendering

* Two-step procedure; interactive cine display using MIP and axial data, the latter for the stenosis grading

† This result considers only the main renal arteries

The imaging parameters might have an impact on the accuracy of CT angiography of renal arteries running parallel to the axial imaging plane. In an experimental phantom study of renal arteries using polyester pipettes filled with iodinated contrast agent and covered with fat and water, a critical renal artery stenosis was best detected with 2 mm collimation, 2-4 mm table increment and 1 mm reconstuction interval (81). For the detection of significant stenosis in the renal artery, the best results were obtained with interpretation of axial images with some of the 3D images (Tables 1 and 2). In addition, the evaluation of accessory renal arteries was most accurate with the interpretation of axial images and MPRs (63). With VR images the accuracy of CT angiography was better and faster than with MIP (115), but the sensitivity of VR interpretation alone (89%) fails to reach same level of accuracy than other studies with the interpretation of various 2D and 3D displays together (Table 2). Secondary signs such as poststenotic dilatation and abnormal nephrogram have shown to be highly specific for significant arterial stenosis (70).

Only one study has been published thus far on the use of MDCT for CT angiography in the detection of atherosclerosis in aortoiliac and renal arteries. In this study, 309 renal arterial segments in 46 patients were evaluated with MIP and VR by two observers. An excellent accuracy of 98% and 99% was shown for the two readers, with sensitivity of 86% and 93% and specificity of 99% and 100%, respectively (118).

CT angiography has an additional benefit in the assessment of the renal artery anatomy and location of the pathology. If the stenosis is locating near the aortic origin, it could be either ostial or truncal, i.e. caused by atherosclerosis of the aortic wall or a true atherosclerostic lesion originating in the renal artery itself (21). The anatomic variations of the renal arteries have been clarified with axial imaging by CT

angiography (119, 120). Thus CT angiography has provided important information on the anatomy and pathological conditions of renal arteries implying benefit for the imaging of renal arteries and for the treatment of renal artery stenosis. Furthermore, in addition to gadolinium-enhanced MRA, CT angiography is useful for the evaluation of living related kidney donors (121). Also other pathological conditions in renal arteries and veins can be evaluated with CT angiography, in addition to diseases of the renal parenchyma and urinary tracts (122). A disadvantage of CT angiography in the imaging of renal arteries is the inability to assess side branches masked partially by the enhancement of the parenchyma. This has particularly been addressed by MDCT, which has improved the spatial resolution and the speed of scanning, allowing better distinction of various phases of the contrast enhancement.

2.2.1.4. CT angiography of carotid arteries

Due to the risks associated with catheter angiography, alternative noninvasive methods, such as noninvasive carotid imaging including CT angiography have been proposed for carotid imaging (123, 124). The advantages of CT angiography are the possibility to evaluate extracranial arteries simultaneously with delineation of soft tissues, including the plaque, and to achieve good spatial resolution in any direction with the three-dimensional display (125). The anatomic orientation of carotid arteries running perpendicular to the imaging plane is favourable for CT angiography (126). The designs and results of various studies of the use of SDCT angiography in the evaluation of carotid arteries are shown in Tables 3 and 4.

The diversity of various elements in CT angiography, including variability in the CT devices, contrast agent infusion implementation techniques, scanning parameters and variable image display for diagnosis, complicates the comparison of various

studies. In addition, the studies had different scales for stenosis grading. However, these studies have proved that CT angiography is a promising tool for the assessment of carotid arteries and the detection of stenoses. The study by Moll et al (123) has in a large study population shown that CT angiography had higher sensitivity than CD-US for the detection of severe (70-99%) stenosis in the carotid artery. In that study the results of various imaging methods were compared with the findings of subsequent surgical operation as a reference. CT angiography was as sensitive and specific as DSA (123).

The multislice technique facilitates rapid scanning of the head and neck, thus allowing either smaller volume high-resolution imaging with isotropic voxel size or imaging of a larger coverage of anatomic areas, i.e. the whole cerebrovascular circulation from aortic arch to intracranial arteries (78) (Figure 2). MDCT has a high resolution in z-direction, facilitating good quality 2D reformats or 3D reconstructions and accurate measurements. In a preliminary study with five patients using MDCT for carotid CT angiography excellent image quality and good demonstration of carotid plaques was reported (144).

2.2.1.5. CT angiography in other vascular territories

A large number of vascular anatomic regions and pathological conditions can be evaluated with CT angiography. Common indications for the examination of the thoracic and abdominal aorta include aneurysm, dissection, penetrating aortic ulcer, atherosclerotic occlusive disease and aortic trauma (145-148). For the preoperative assessment of abdominal aorta and iliac arteries for the treatment of an aneurysm by endovascular placement of a stent-graft, CT angiography is a reliable method for the imaging of vascular anatomy and pathology. Some automated measurement

methods are available for the precise assessment of various dimensions and distances that are important for the planning of treatment (149-152). In addition, the follow-up of the aorta and iliac arteries after surgical or endovascular treatment with CT angiography is reliable revealing possible complications (153-155).

MDCT has several advantages compared over SDCT in the evaluation of the aorta and iliac arteries (156). In the initial stage of CT angiography, the imaging of aorta and its branches was performed with 3 mm collimation and table feed leading to 9 cm of anatomic coverage and the display of arterial branches up to the second- to fourth-order (65). Even with four-channel MDCT the entire abdominal circulation could be examined with 1 mm collimation, allowing visualisation of several visceral arterial branches and the enhanced bowel wall (89). In addition, lower extremity arterial inflow and runoff seems to be a new indication of CT angiography with modern MDCT technique (157). In the study of Ota et al. (158), the diagnostic accuracy of MPR was excellent compared with the moderate accuracy of axial source MDCT images to evaluate stenoocclusive segments in lower limb arteries. Contrast CT has shown to be superior to MR angiography in the imaging of most intravascular stents except tantalum stent (159).

The advent of CT angiography has changed the diagnostics of acute pulmonary embolism dramatically. MDCT enables the accurate evaluation of the pulmonary arteries down to the fifth order (160). CT angiography is also feasible for the diagnosis and posttreatment follow-up of vessel anomalies and arteriovenous malformations in adults and children (161-163).

In the evaluation of patients suffering from subarachnoid haemorrhage CT angiography of intracranial arteries performed immediately after detection of a haemorrhage in nonenhanced CT has been shown to detect most aneurysms with

certainty and retrospectively assessed most aneurysms could have been operated based on CT angiography alone (164, 165).

Motion artefacts have been a problem for CT angiography, especially in thoracic imaging due to pulsation and motion of the heart. Artefacts are pronounced with 360° linear interpolation algorithm (166). These artefacts have been reduced with faster scanning, firstly with the advent of subsecond scanners (167) and secondly with MDCT technique, but the motion artefacts due to pulsation did not completely disappear (168). The use of ECG gating has improved the imaging of thoracic vasculature.

A quite new and rapidly developing indication for CT angiography in the era of MDCT with ECG gating is the evaluation of coronary arteries (169-171). The accuracy of ECG-gated CT angiography to detect stenosis in the coronary artery has been best for the main arteries (172). Conventional CT and electron beam CT are useful for the detection of the coronary artery calcifications (173).

Table 3. The design of SDCT angiography studies on carotid arteries

Study	Contrast media				Imaging parameters					Reformat or reconstruction used for the diagnosis
	Volume ml	Concentration mg I/ml	Flow rate ml/s	Bolus triggering* (s)	Collimation/Slice thickness mm†	Feed mm	pitch	Incr. mm	Tube Current	
Schwartz, 1992 (62)	75	(60%)	2.5	- (20)	4/4 (n=10) 2/2 (n=10)	4 2	1	2	125 kVp 165 mA	SSD
Dillon, 1993 (127)	120 (90 – 140)	350	1.8 (1,4 –2.0)	- (35)	3/3	3	3	3	120kV 250 mAs	SSD
Marks, 1993 (128)	90	300	3	- (15)	2 or 3/NA	3 2	1 1	1	NA	MIP+axial‡
Cumming, 1994 (129)	100 – 120	(60% nonionic)	2 – 2.5	- (24)	2/NA	2	NA	1	120kV 165mA	Interactive SSD+MPR
Leclerc, 1995 (130)	90	300	3	- (20)	2/NA	3	1.5	1	NA	Axial, SSD, MIP
Link, 1995 (131)	100	270	3	- (12)	2/1	2	1	1	120kV 210 mAs	SSD
Tarjan, 1996 (132)	150 – 250	150	2	- (20)	3/NA	NA 12 scan/min velocity with a total scanning time of 2-3 min	NA	NA	120 kV 170 mA	Axial, SSD, MIP, integral,ray-sum
Papp, 1997 (133)	100	(30 g iodine)	1.5	- (30)	3/NA	3	1	2	120 kV 250 mA	SSD, interactive SSD+axial
Magarelli, 1998 (134)	80	350	3	+ (15-22)	3/NA	3	1	NA	120 kV 160 mAs	Interactive MIP+axial
Cinat, 1998 (135)	125	370	2.5 – 3	- (12)	2/2	NA	1.25	2	NA	Interactive MIP+axial
Leclerc, 1999 (136)	120	350	3	- (20)	2/NA	2	1	1	120 kV 220 mA	Axial, VR, MIP
Marcus, 1999 (137)	140	300	3.5	NA(15-26)	3/NA	3	1	1.5	120 kV 210 mAs	VRT,SSD
Sameshima, 1999 (138)	90	300	3-4	-(15-25)	3/NA	3 – 4	1 – 1,5	1	120 kV 210 mA	MIP

Verhoek, 1999 (139)	100	350	3	+	NA/2	3	1,5	1	120 kV 240 mA	MIP, VR,t-CT
Anderson, 2000 (140)	120	300	3	+	3/1	NA	1,5	NA	120 kV 200 – 320 mA	Axial, MIP, SSD
Binaghi, 2001 (141)	100	300	NA	-(13-15)	3/3	3	1	1	120 kV 200 mA	Interactive axial+MPR+MIP
Moll, 2001 (123)	120	300	2,5 – 3.0	±(15,18,20)	2/NA	3	1,5	1 or 2	140 kV 140 mA	Interactive axial+SSD+VR+MIP
Randoux, 2001 (142)	140	250	2.5	+	3/1	3	NA	1	NA	Interactive axial+oblique MPR
Alvarez-Linera, 2003 (143)	150	NA	3	+	2/NA	2	1	NA	120 kV 210 mA	Interactive MIP + SSD +axial‡ + multiplanar rendering reconstructions‡

Note – NA, not available; HU, Houndsfield unit; MIP, maximum intensity projection; SSD, shaded surface display; VR(T), volume rendering (technique); MPR, multiplanar reformation; t-CT, transverse 2D-CT

* The fixed delay time in parenthesis

† The width of collimation and reconstructed slice thickness have probably the same value

‡ Those images used only for calcified stenoses

Table 4. Diagnostic performance of carotid SDCT angiography in comparison to conventional angiography: A review of the literature

Study	n vessels (patients)	Evaluation method for the degree of stenosis	Scales for grading	Criteria for the significant finding	Results				
					Sensitivity %	Specificity %	Overall accuracy %	Agreement %	Other result
Schwartz, 1992 (62)	40 (20)	Visual estimation	4		NA	NA	NA	92	
Dillon, 1993 (127)	54 (27)	Visual and measurement of the DSD	4		NA	NA	NA	82	κ=0.856
Marks, 1993 (128)	28 (14)	Measurement of the DSD	4		NA	NA	NA	86	r=0.921
Cumming, 1994 (129)	70 (35)	Measurement of the DSD	5		NA	NA	NA	NA	r=0.928
Leclerc, 1995 (130)	39 (20)	Measurement of the DSD	6		NA	NA	NA	95	Axial κ=0.94, r=0.935 MIP κ=0.96, r=0.856 SSD κ=0.77, r=0.809
Link, 1995 (131)	80 (44)	Measurement of the DSD	4		NA	NA	NA	65	Agreement of 36-64-68% in three stenosis categories
Tarjan, 1996 (132)	30 (15)	Measurement of the DSD	4		NA	NA	NA	97–59–66–62–66[†]	
Papp, 1997 (133)	96 (48)	"Evaluation of the degree of stenosis"	5	> 70%	SSD 65–66 [‡] SSD+axial 76–80[‡]	NA	NA	NA	Mean error: SSD f[1.93]=5.98 SSD+axial images f[1.93]=0.00
Magarelli, 1998 (134)	40 (20)	Measurement of the DSD	5	> 70%	81.4	96.4	91.3	NA	
Cinat, 1998 (135)	106 (53)	Measurement of area reduction		>80%	87	90	89	NA	NPV 88%, PPV 89%
Leclerc, 1999 (136)	44 (22)	Measurement of the DSD	5	>70%	Axial 67 MIP 86 VR 100	Axial 96 MIP 91 VR 92	NA	NA	Axial κ=0.90 MIP κ=0.87 VR κ=0.85
Marcus, 1999 (137)	46 (23)	Measurement of the DSD	4	≥70%	VRT 89–94[§] SSD 88–94[§]	VRT 96–97[§] SSD 93 [§]	NA	NA	Interobserver agreement (κ): VRT 0.90 – 0.97 SSD 0.95 – 0.97

Sameshima, 1999 (138)	128 (64)	Estimation of the DSD	5		NA	NA	NA	NA	r=0.987
Verhoek, 1999 (139)	38 (19)	Measurement of the DSD	4		NA	NA	NA	VR 76 MIP 71 t-CT 89	VR κ=0.67 MIP κ=0.62 t-CT κ=0.85
Anderson, 2000 (140)	80 (40)	Measurement of the DSD	5	> 50%	Axial 89 MIP 90 SSD 85	Axial 91 MIP 82 SSD 86	Axial 90 MIP 86 SSD 86	NA	PPV Axial 86% MIP 78% SSD 75% NPV Axial 93% MIP 93% SSD 90%
Binaghi, 2001 (141)	49 (25)	Measurement of the DSD	4	≥ 70%	89	100	NA	NA	PPV 100%, NPV 94% κ=0.94
Moll, 2001 (123)	356 (178)	Measurement of DSD and area stenosis with reference to surgery	3	≥50%	98.3	100	NA	NA	
Randoux, 2001 (142)	44 (22)	Measurement of the DSD	6	> 70%	100	100	NA	NA	r=0.93 Interobserver κ=0.92
Alvarez-Linera, 2003 (143)	80 (40)	Measurement of the DSD	5	≥ 70%	74.3	97.6	NA	NA	κ=0.72 Pearson correlation=0.86

Note – NA, not available; κ, statistic kappa; r, Spearman's correlation; DSD, diameter stenosis degree; MIP, maximum intensity projection; SSD, shaded surface display; VR(T), volume rendering (technique); PPV, positive predictive value; NPV, negative predictive value

* Only stenotic arteries included in the analysis

† Values for each image display respectively in the same order as in the Table 3

‡ The approximation of values from the bar chart done by the author (MB)

§Minimum and maximum values for three different observers

2.2.2. Angiography

2.2.2.1. Digital subtraction angiography

DSA provides advantages compared with the older cut-film technology such as the use of smaller diameter catheters and the road mapping technique for tortuous arteries (174). The biplane equipment facilitates further to decrease the amount of contrast material in carotid arteries (175). The use of nonionic contrast material reduces side-effects. Usually the arterial puncture is performed in the groin, and the Seldinger technique is used through the femoral artery for the cathetrisation for both carotid and renal arteries. Selective catherisation of both carotid and renal arteries allows better enhancement in the target vessels and good spatial resolution. Multiple projections are needed to properly visualise the main arteries and the branches of the renal arteries. Alternative access via radial, brachial or axillary artery can be used, if the transfemoral route is not available. Direct puncture of carotid artery can also be done, but there is a considerably higher risk for local complications (175).

In carotid arteries, there is a risk for stroke and minor complications caused by angiography procedure. Willinsky et al. (124) found a complication rate of 1.3% in 2899 consecutive patients, of which 0.5% had permanent sequelae. The procedural risk is increased in patients suffering from atherosclerosis (176). In addition, silent embolism detected with MRI after diagnostic angiography was shown to be common among patients with vasculopathy (177). In that study patients with silent embolism needed more contrast medium, longer fluoroscopy time, more frequent additional catheters and had more vessels that were difficult to probe (177). Due to the risks associated with angiography, alternatives such as the use of noninvasive carotid imaging have been proposed, especially for the screening of carotid stenosis (124).

The resolution of intravenous DSA is less than that of arterial DSA, and noninvasive imaging methods have almost totally replaced the use of intravenous DSA. Although noninvasive imaging methods are suitable for many patients in primary diagnosis, arterial angiography is still the 'gold standard' with which other imaging modalities are compared. Arterial angiography is important procedure preceding invasive interventions. As an adjunct to angiography, the pressure measurement cross the stenosis provides additional information about the haemodynamic significance of RAS (178).

2.2.2.2. Rotational angiography

The rotating angiography system was introduced in 1975. Several improvements have enabled its use for clinical purposes, for example imaging of intracranial aneurysms before interventions (179). The imaging procedure is performed using angiography equipment with a rotating C-arm doing two 200° sweeps, the first one is the mask and the second is with contrast media injection into the target vessel (179). The patient must lie motionless during the procedure. The total number of images depends on the speed of the rotation and the frame rate used for the imaging, varying between 50 and 140. Rotational angiography with multiple projections provides benefit over DSA in vascular imaging (180).

Rotational angiography has shown to be more accurate than DSA to determine the narrowest diameter in a stenosed carotid artery (181, 182). A recent advancement in rotational angiography is a 3D modality. With this technique the conversion of the two-dimensional angiographic data to cross-sectional images is possible, facilitating the measurement of the cross-sectional area of a normal or stenosed artery. Three-dimensional views of rotational angiography including SSD, MIP, VR and MPR

provide excellent visualisation of vasculature. The possibility of true stereo images increases the clinical benefit of rotational angiography (179). For native and transplant renal arteries rotational angiography can be used to find the optimum projection, showing the orifice of the native artery with varying angles in relation to the aorta, or anastomosis area of a transplant artery (183).

2.2.3. Magnetic resonance

2.2.3.1. Magnetic resonance imaging

Magnetic resonance imaging (MRI) facilitates the imaging of atherosclerotic lesions in the artery wall properly because of its excellent soft tissue contrast. Due to the favourable position of carotid artery and the predisposition to considerably large, advanced atherosclerotic lesions, carotid region has been widely studied using MRI. The location and characteristics of the atherosclerotic lesion can be evaluated with MRI, in addition to measurement of lesion size and the vessel wall thickness. In early studies using spin-echo sequences different components of plaque could be distinguished. With the combination of T1 and T2 weighted images, the identification of atheromatous core, collagenous cap, calcifications, media, adventitia and perivascular fat seemed to be possible (184-186). The black blood MRI technique has proved useful in the assessment of plaque burden (187). With a lipophilic contrast agent (gadofluorine) it may be possible to image early atherosclerotic changes more widely with MRI, as shown in an animal study using Watanabe heritable hyperlipaemic rabbits (188).

The vulnerability of the plaque has been an object of several studies. In the study by Hatsukami et al. (189) there was a good correlation for distinguishing intact, thick fibrous from intact, thin and disrupted caps in atherosclerotic human carotid arteries

in vivo with MRI using a 3D multiple overlapping thin slab angiography protocol. MRI with a multispectral protocol (T1, T2, and proton density-weighted images combined with 3D time-of-flight (TOF) imaging), the lipid rich necrotic core of human carotid atherosclerosis has proved to be detectable with high sensitivity and specificity (190). TOF images helped to identify intraplaque haemorrhage from the lipid core. However, the heterogenous signal of a complex atheroma on MRI degrades the capability of high resolution multispectral MRI to stage intraplaque haemorrhage (191). The neovasculature of carotid artery atherosclerosis has been studied with dynamic contrast-enhanced MRI (192).

Direct imaging methods for the detection of vulnerable plaque with haemorrhage or thrombus have been developed. The MRI technique with direct thrombus imaging shows pathology as high signal of methaemoglobin compared to suppressed background (193). MRI with infusion of superparamagnetic particles of iron oxide has shown them to concentrate in atherosclerotic plaques by phagosytosis of magrophages in animals (194). In addition, molecular imaging with fibrin-targeted paramagnetic nanoparticles may offer one possibility for the detection of vulnerable plaque (195).

2.2.3.2. Magnetic resonance angiography

There are several methods for performing MR angiography (MRA). In clinical practise, the most recent method based on the use of contrast media, i.e. contrast-enhanced MRA (CEMRA), and the methods based on flowing blood i.e. TOF and phase-contrast (PC) techniques are the most often used (196). Flow-based techniques are totally noninvasive and safe for the patients. CEMRA with intravenous injection of gadolinium-based contrast agent is minimally invasive, and contrast agent

seldom induces adverse effects. However, there are also contraindications for MRA as well as other MR studies, including claustrophobia, lack of co-operation, and the presence of a pace maker or ferromagnetic metallic foreign bodies in the patient.

The flow-based sequences use different ways to produce angiographic images with 'bright' vessels (197). The TOF method first has a pulse sequence with a short repetition time for the saturation of stationary background tissue. The saturation of the spins in the protons of the blood also occurs, but in the flowing blood the saturated protons are displaced by blood flow with nonexcited protons before a receiving pulse, allowing flow-related enhancement (in-flow effect). The use of a downstream saturation band eliminates the venous enhancement in arterial imaging. The carotid arteries parallel to the z-axis of MR equipment are well suited for TOF imaging. Both 2D and 3D methods have been used for the carotid MRA TOF imaging (198, 199). In the phase-contrast method the signal of flowing blood is based on the phase shift of the moving spins. Phase encoding is essential with this technique (196). The phase-contrast method allows flow quantification, which provides important information for the significance of carotid stenosis (200).

Flow-based methods have some disadvantages. Both TOF and PC methods suffer from a limited field of view. The flow-related signal is susceptible to disturbances of the laminar flow, leading to overestimation of the stenosis and inaccuracy in distinguishing a near occlusion from a total occlusion, especially with the TOF technique. The PC technique is not susceptible to slow flow artefacts, but the long examination time is a disadvantage.

In CEMRA using gradient echo imaging, the T1 relaxation time shortening of blood is accomplished with intravenously infused contrast media, and the signal is independent of the flow phenomenon. There are several techniques of CEMRA, but

the main technique used is gradient-echo sequence using first-pass of contrast media. The short acquisition time of CEMRA allows dynamic imaging with a wide field of view, which enables imaging of the whole carotid circulation (201). Alternatively, various techniques for the detection of contrast inflow can be used for optimising the contrast enhancement in target vessels, i.e. test bolus or bolus triggering, providing advantages for the selection of imaging parameters and resolution (202). Technical development of MR devices permits whole body MRA studies suitable e.g. for the evaluation of patients suffering from claudication (203). Furthermore, dynamic MR imaging with a contrast agent has the potential to evaluate kidney function, providing supplemental information to that of renal MRA (204). For the assessment of carotid stenosis, the CEMRA has been stated to be a reliable method (143, 205), but whether MRA should replace conventional angiography is still controversial (201) as is the case for all noninvasive imaging methods (206).

2.2.4. Ultrasound

2.2.4.1. Grey Scale Imaging

High-resolution grey scale imaging with a B-mode is suitable for the evaluation of atherosclerotic lesions in the artery wall of superficial arteries such as carotid, brachial and femoral arteries. Transesophageal echocardiography enables the imaging of atherosclerosis in the aortic wall (207). With grey scale imaging it is possible to assess the extent of atherosclerosis in extracranial carotid arteries, the severity of the lesions and plaque characteristics such as echogenicity (low, moderate, high) or homogenous versus heterogeneous plaque morphology (208). Echolucency (low echogenicity) of the plaque measured with quantitative computer-assisted index has been shown to increase the risk of stroke in carotid stenting (209).

In addition, heterogeneity of the carotid plaque representing the intraplaque lipid core or haemorrhage has been shown to correlate with symptoms better than any degree of stenosis (210). In ultrasound studies, mural calcification in the plaque with acoustic shadow limits the visualisation. The thickness of intima-media complex in the carotid artery is often used as a marker of atherosclerosis (211). The measurement of the intima-media complex is operator dependent and may have a low reproducibility. However, the use of a trained sonographer has provided reliable results (7, 211).

2.2.4.2. Colour Doppler ultrasound

CD-US of flowing blood is based on the Doppler effect. The Doppler frequency is defined as the difference between the received and transmitted frequencies, and the detected Doppler frequency is strongly influenced by the Doppler angle (212). A change in the echo signal of moving objects (i.e. red blood cells) relative to the transducer expresses the direction of the flow. Pulsed Doppler is more often used for clinical vascular imaging. Doppler signal frequency reflects the spectrum of velocities in the scanned area. In colour ultrasound, the direction of the flow related to the transducer is expressed with different colours and the spectrums of frequencies (mean velocity) are displayed with different colour shades. The colour image data is superimposed on B-mode data (212). In Doppler waveform spectra analysis, the angle-corrected data should be recorded in the stenosis area. Optimal baseline velocity scaling prevents the most common artefact '"aliasing" in Doppler imaging (212).

The grey scale US study combined with CD-US using meticulous instrumentation is a useful tool for the assessment of atherosclerosis and stenosis of the carotid bifurcation region (213). Screening of carotid stenosis in symptomatic patients with

CD-US is relatively inexpensive and totally noninvasive. In one study the use of contrast agent has increased the accuracy of CD-US in separating near-occlusions from total occlusions (214). However, the variation between different laboratories and the use of different diagnostic criteria for the diagnosis has limited the value of CD-US as a single method on which to base the treatment decision of carotid stenosis (215, 216). Recently, a consensus statement made by multidisciplinary panel of vascular ultrasound specialists for carotid US with recommendations for the diagnostic criteria and reporting system have been published (217).

CD-US of renal arteries with waveform analysis of the Doppler spectrum of the intrarenal renal artery branches can be used for selected patients potentially having renal artery stenosis. CD-US has some limitations for the assessment of renal artery stenosis, such as limited visualisation of the renal artery deep in the abdominal cavity, the prevalence of renal accessory arteries and the variability to interpret the intrarenal spectrum of Doppler waveforms sometimes affected by other renal diseases (218).

2.2.4.3. Intravascular ultrasound

Intravascular ultrasound (IVUS) is mainly used as an adjunct to angiography due to invasiveness of IVUS, in which the imaging catheter is placed inside the artery. There are two types of probes incorporated into the imaging catheter. The probes are usually sideward looking. One type has a mechanical rotating single-element catheter tip, and the other type has electronically switched phase array catheter tip (219). The imaging catheter is placed in the target artery using a guide wire. During the scanning procedure, the catheter tip is pulled backwards either manually or using

a motorised pull-back manoeuvre (219). Excellent axial resolution is obtained using high ultrasound frequencies (20 to 50 MHz) (220).

IVUS produces real-time tomographic images from the entire circumference of the artery, revealing all wall components and the extent of atherosclerotic disease, unlike angiography, which depicts only the stenosed part of the diseased vessel in a silhouette image. Therefore, with IVUS it is possible to image all the atherosclerotic segments of the imaged artery, even when the lumen size has not decreased due to positive remodelling. As in conventional ultrasound, the morphology of the atherosclerotic plaque is characterised as hypoechoic, hyperechoic or "mixed" lesions (221). The arterial lumen, atheroma and area stenosis can be measured from the 2D IVUS images. A relatively new 3D IVUS imaging produced by computerised reconstruction of serial tomographic images allows the quantification of plaque volume (219). Plaque calcification causes acoustic shadowing, which hides the arterial wall structures behind the calcification. Another disadvantage of IVUS imaging is that penetration of the high frequency ultrasound is less optimal in large-diameter arteries such as the carotid bulbs (221).

IVUS imaging is widely used in coronary arteries, providing new insights in the diagnosis and therapy of coronary artery disease (220). IVUS has proved to be safe and informative also for the imaging of carotid arteries with a mild stenosis (221). IVUS imaging has a great value in the pre- and postprocedural evaluation for endovascular treatment (222).

2.2.5. Nuclear medicine and other methods for the investigation of atherosclerosis

Scintigraphy with the angiotensin-converting enzyme inhibitor captopril or 'captopril renography' evaluating technetium-99m-diethylenetiamine penta-acetic acid (DTPA) uptake in kidneys is a noninvasive method for the screening of RAS (223). Positive results from captopril renography are determined by decreased relative uptake of DTPA, with 1 kidney accounting for less than 40% of the total glomerular filtration rate and delayed peak uptake of DTPA of more than 10-11 minutes (normal is 3-6 min). Renography performed before and after oral captopril enables the observation of captopril-induced change in renogram, which finding is highly specific (224). Captopril renal scintigraphy is influenced by renal parenchmal disease, postrenal obstruction and has poorer ability to discover bilateral RAS than unilateral RAS.

Nuclear scintigraphic imaging with radiolabelled lipoproteins and platelets also enables the characterisation of some the features of the atherosclerotic plaque and adjacent thrombus, but the limitations are poor target/background and target/blood ratios (225). New tracers such as radiolabelled peptides, antibody fragments and metabolic tracers for nuclear scintigraphic imaging have been and will be further developed (225). A specific protein (annexin V) radiolabelled with technetium enables the detection of cells prone to apoptosis, probably indicating the vulnerability of the plaque (226). In a recent human study, positron emission tomography (PET) using fluorine-18-labeled fluorodeoxyglucose as a radiotracer for the estimation of glucose metabolic activity, i.e. FDG-PET, seems to be an interesting tool for the detection of the metabolic activity of atherosclerotic changes (227).

IVUS imaging can be combined with intravascular elastography, in which the local strain of the tissue (plaque) is displayed with an elastogram as an adjunct to the

IVUS image. Intravascular elastography has been stated to reveal plaque vulnerability, defined as a plaque with a high-strain region adjacent to low strain regions (228). Other intravascular modalities for the detection of vulnerable plaque include angioscopy, thermography, optical coherence tomography, Raman spectroscopy and NIR spectroscopy (229). Intravascular methods to characterise the plaque components can be combined with IVUS imaging, thus yielding both anatomic and, to some extent, functional information.

3. AIMS OF THE STUDY

The aim of the study was to verify the reproducibility and accuracy of CT angiography for the detection of atherosclerosis in renal and carotid arteries and for the quantification of atherosclerotic stenosis.

The specific aims were as follows:

1) To evaluate SDCT angiography with various diagnostic algorithms as a screening method for RAS and to evaluate the usefulness of renal cortical enhancement measurements as an adjunct to CT angiography for RAS diagnosis (Study I).

2) To evaluate the ability of SDCT angiography to detect atherosclerosis of the carotid arteries in comparison with 3D TOF MRA, using DSA and IVUS as references (Study II).

3) To evaluate the diagnostic performance and reproducibility of MDCT angiography with interactive interpretation (visual estimation and manual MPR measurements) and automated 3D CT angiography analysis software for the assessment of carotid artery stenosis compared with rotational angiography and DSA as standards of reference (Studies III and IV).

4. PATIENTS AND METHODS

4.1. STUDY DESIGN

4.1.1. Approval of the Ethics Committee

The study protocols were approved by the ethical committee of Kuopio university hospital. Informed consent was obtained from all the patients.

4.1.2. Study subjects

In this study have been enrolled altogether 104 patients for four studies.

4.1.2.1. Patients with RAS or suspected renovascular hypertension (Study I)

Thirty-seven patients (20 males and 17 females, mean age 66 years, range 28-81) who underwent DSA of the abdominal aorta and renal arteries between August 1994 and February 1997 were included in this first study, and SDCT angiography was performed for all patients. The indications for DSA were claudication or chronic pedal ulcer (n=26), clinically suspected RAS (n=6), evaluation of abdominal aortic aneurysm or iliac pseudoaneurysm (n=3), clinically suspected vasculitis (n=1) and clinically suspected chronic intestinal ischaemia (n=1).

Among the 78 renal arteries, there were 10 accessory renal arteries in DSA included in the study. Two renal arteries were excluded because of unacceptable superimposition on the aorta in nonselective DSA. Three arteries were excluded because of problems in the timing of contrast media injection or poor patient co-operation during CT angiography.

4.1.2.2. Patients with carotid atherosclerosis (Study II)

During the period 1995-1998, selective carotid DSA and SDCT angiography was performed for 31 patients (23 males and 8 females), and 3D TOF MRA was performed for 21 of these patients. The indications for DSA were transient ischaemic attack (n=12), amaurosis fugax (n=5), hemispheric stroke (n=3), convulsion (n=1) and in ten cases DSA was primary investigation before intracranial endovascular intervention.

IVUS imaging and selective carotid DSA were performed on one carotid artery of ten patients in connection with various intracranial and extracranial endovascular interventions, including embolisation of arteriovenous malformations (n=4) or cerebral artery aneurysms (n=3), intracranial balloon angioplasty (n=2), and stenting of the proximal internal carotid artery (n=1).

4.1.2.3. Patients with cerebrovascular symptoms (Studies III -IV)

Both DSA and MDCT angiography were performed for 36 consecutive patients between September 2001 and June 2002. Demographic data of the patients and indication for carotid angiography are given in Table 5.

TABLE 5. Clinical Characteristics of the Patients (*n*=36) of Studies III and IV

	n	%	Mean	Range
Men	21	58		
Women	15	42		
Age (years)			68	50 - 83
Associated diseases				
No associated disease	2	6		
Diabetes	10	28		
Hypertension	18	50		
Cardiovascular disease	17	47		
Hypercholesterolaemia	17	47		
Other	21	58		
Previous endarterectomy	2	6		
Duration of neurological disorders (months)			7.9	0.2 - 72.0
Indications for the imaging				
Transient ischaemic attack	14	39		
Amaurosis fugax	9	25		
Minor hemispheric stroke	13	36		

4.2. METHODS

4.2.1. Digital Subtraction Angiography

For the studies I and II, intra-arterial DSA studies were performed using Siemens Polytron angiography equipment (Siemens Medical Engineering Group, Erlangen, Germany). For the III and IV studies, selective angiography was performed using biplane DSA equipment (Siemens Neurostar Plus, Forchheim, Germany).

Renal DSA was performed via the transfemoral approach, except for two patients, who were studied via the transbrachial approach. A 4 F or 5 F pigtail catheter was placed in the proximal abdominal aorta, and 25-30 ml of contrast media was injected at a rate of 18-22 ml/s. Selective renal angiography was also performed in 6 cases of clinically suspected RAS. Anteroposterior and appropriate oblique views to visualise the whole length of the renal arteries were obtained.

Contrast angiography studies for carotid arteries (Studies II-IV) were performed with at least two projections (Study II) or with four projections including anteroposterior, lateral, ipsilateral oblique and contralateral oblique projections (Studies III-IV). Each carotid artery was imaged with 5-6 ml of nonionic contrast media (Visipaque 270mgI/ml, Nycomed, Oslo, Norway) per injection and a flow rate of 8ml/s. In addition, the aortic arch and subclavian arteries were imaged. The images were displayed and processed on a monitor with a 1,024 x 1,024 matrix (studies III-IV).

4.2.2. Rotational Angiography (Studies III-IV)

For rotational angiography, the patient was positioned in the isocenter of the angiography equipment. For enhanced rotation imaging, 23 ml of contrast media was injected at a flow rate of 2.5 ml/s into the common carotid artery. After contrast media injection, the imaging started in a lateral position with 180° rotation in 8 seconds around the carotid bifurcation to acquire 80 projections. A 512 x 512 image intensifier matrix was used.

For the measurement of the diameters of the carotid lumen and the degree of stenosis on rotational DSA, both MPR technique and the 80 original angiography images were used. The site of maximal stenosis, and the reference point distal to the

carotid bulb were determined. The shortest diameters at the maximal stenosis point and the diameter at the reference point were used to calculate the stenosis degree according to the NASCET criteria.

4.2.3. SDCT angiography of renal arteries (Study I)

SDCT examinations were performed with a Siemens Somatom Plus scanner. Unenhanced orienting slices of the abdominal aorta and kidneys were first obtained at 10 mm collimation. The contrast media (Ultravist 300 mg I/ml Schering, Germany or Iopamiro 300 mg I/ml, Astra Tech, Sweden) was administered with a power injector at a flow rate of 4 ml/s via an 18 gauge cannula placed in the antecubital vein. A test bolus of 12 ml was injected for optimising the scan delay time, which was installed from the time of peak aortic enhancement at the level of the superior mesenteric artery, minus three seconds. The contrast material volume for the spiral scan was 150 ml. Spiral scanning began at the level of the superior mesenteric artery (collimation 3 mm, table feed 3 mm per second, tube current 165 mA with 120 kV). Axial images were created with the standard reconstruction kernel and 180° linear interpolation algorithm. The table increment for the axial slices was 1 mm.

The MIP and MPR images were created on a workstation (Diagnostic reporting console, Siemens, Germany). First, the main renal and possible accessory renal arteries were located using the cine mode. For the MIP reconstructions, bone structures and enhanced renal veins were removed from the axial slices with a 3D slab editing program. MIPs were reconstructed at various angles around the z-axis, and 3-5 images of each renal artery were recorded on film. In the case of complex renal artery anatomy, additional MIP views around the x-axis were also created. Oblique (based on axial and coronal reference images) MPRs were done

interactively for each renal artery stenosis or wall calcification discovered in the MIP images, and also for each renal artery ostium. All MPR images were recorded on film. The window settings were selected patient by patient.

The films were read independently by two radiologists in two separate sessions: 1. MIP images alone 2. MIP and MPR images together. The degree of RAS was assessed as follows: grade I = 0% - 49% stenosis, grade II = 50% - 74% stenosis, grade III = 75%-99% stenosis, grade IV = occlusion. A stenosis degree of $\geq$ 50% was considered to be haemodynamically significant. Calcifications were registered from the MIP images and classified into three categories: 0 = no calcifications, 1 = calcifications not disturbing stenosis degree assessment, 2 = calcifications disturbing stenosis degree assessment. One observer read the films twice with an interval of one month.

The degree of renal artery diameter stenosis from the DSA films and, after a two-month interval, from the MIP and MPR films was measured by one observer using a digital micrometer. All measurements were performed using a magnifying-glass film viewer at approximately threefold magnification. Because the stenosis degree of heavily calcified lesions could not be measured from the MIP images, they were all considered to be haemodynamically significant (six segments).

4.2.4. Measurement of renal cortical enhancement (Study I)

All patients who had multiple renal arteries to a single kidney were excluded, leaving 26 patients for this part of the first study. The renal cortical enhancement values were measured from 5 axial slices from the middle of the imaging volume. The highest and lowest values were excluded, and the mean value was calculated from the remaining three values. The ratio of the enhancement values for the two kidneys

was calculated, and the result was compared to the difference in renal artery stenosis degrees.

4.2.5. Three-dimensional TOF MRA of carotid arteries (Study II)

Three-dimensional TOF MRA was performed at 1.5 Tesla (Siemens Magnetom SP4000 and Vision) with a neck coil. Axial 3-D TOF MRA acquisitions with 64 partitions (repetition time 33 ms, echo time 8.0 ms, flip angle 20°, 1 signal average, effective slice thickness 0.8 to 1.5 mm, field of view 200 mm, 256x512 matrix) were performed covering both the carotid bifurcations. Acquisition time for 3D TOF MRA was 5-9 minutes.

4.2.6. Intravascular ultrasound of carotid arteries (Study II)

IVUS was performed with a 3.5-F, 30-MHz imaging catheter (Sonos; Hewlett Packard, Andover, Mass.) using a mechanical transducer (Medi-tech/Boston Scientific, Watertown, Mass.) through a 7F multipurpose or right coronary guiding catheter. Using digital road mapping control, the IVUS catheter was introduced into the internal carotid artery (ICA) over a 0.018-inch guide wire. Imaging was registered on a super-VHS tape while the catheter was slowly pulled backward manually from the ICA to the proximal part of the common carotid artery. Gentle manipulation of the catheter was applied to keep the probe positioned as centrally as possible. To register the exact location of the probe within the artery, 7 to 10 single radiographs were obtained in the same projection during the imaging, and the corresponding time points were marked with annotations in the IVUS videotape for the determination of the longitudinal position of the individual axial levels of IVUS with reference to the level of the carotid flow divider. Stenotic lesions were registered. Intralesional areas

with brighter echogeneity than the reference adventitia and clear acoustic shadowing were interpreted as calcified. The measurements were obtained at a single freeze video image during the systolic phase, and the reference diameter was measured from the outer edge of the media layer. Luminal diameters and thickness of the plaque were also measured.

4.2.7. CT angiography of carotid arteries

4.2.7.1. SDCT angiography (Study II)

SDCT angiography examinations were performed with a Siemens Somatom Plus scanner using the following parameters: tube current 165 mA with120 kV, 2 mm collimation, and 3 mm table feed. Nonionic contrast medium containing 300 mgI/ml (Ultravist, Schering, Germany or Xenetix, Guerber, France) was administered with a power injector (Angiomat CT, Liebel Flarsheim Co.,OH) via an 18 gauge cannula placed in the antecubital vein. A volume of 80-100 ml was injected at a flow rate of 3-4 ml/s. The scan delay time was established with a test bolus of 12-15 ml of contrast medium. Spiral scanning was started at the level of the sixth cervical vertebra, and reached the skull base. Patients were allowed to continue quiet breathing during scanning, but they were asked to avoid swallowing and moving. Axial images were created with the soft reconstruction kernel and 180° linear interpolation algorithms, and images were reconstructed every 1 mm. All axial images were recorded on film. The scanning time was 30-40 seconds.

4.2.7.2. MDCT angiography (Studies III-IV)

MDCT angiography was performed with a four-channel multidetector-row Siemens Volume Zoom CT device with 120 kV and 250 mAs. The other imaging parameters

were 1 mm collimation, 5 mm/s table feed and 0.5 s gantry rotation time. The contrast agent (Ultravist 300 mgI/ml, Schering AG, Berlin, Germany) volume for CT angiography was 80 ml with a saline chaser bolus of 30 ml using a flow rate of 3 ml/s via an 1.3 mm (18G) cannula through the antecubital vein. The bolus triggering method was used for the assessment of the optimal time delay for CT scanning to optimise the contrast enhancement in carotid arteries, and the ROI indicator was placed on a reference image obtained from the aorta. The scanning started 5 s after the enhancement in the aorta reached 70 HU. Spiral scanning included the volume between the sixth cervical vertebra and the circle of Willis. The patients were asked to breathe evenly and smoothly without swallowing or moving. The raw data of CT angiography was routinely reconstructed to axial slices with a soft tissue algorithm and a section thickness of 1.5 mm using a 1.0 mm reconstruction interval.

4.2.8. Assessment of carotid artery stenosis

4.2.8.1. Visual interpretation (Studies II-IV)

In the study II, the imaged portion of the extracranial carotid artery was divided into four segments: (1) the ICA above the bulbar area, i.e. the distal ICA; (2) the ICA bulb (in cases without unequivocal anatomic bulbar widening, the ICA bulb was defined as covering a segment 0-20 mm above the flow divider); (3) the carotid bifurcation 0-10 mm below the flow divider; and (4) the common carotid artery 10 to 50 mm below the flow divider. The SDCT angiography axial source images were independently reviewed by a radiologist experienced in CT angiography and a vascular radiologist. Atherosclerotic lesions were registered, and the diameter stenosis degree on each segment was visually estimated.

In the Studies III and IV, the axial images were loaded on a separate workstation (ADW 4.0, GE medical systems, Milwaukee, USA) for further analysis. A window width of 700 and window level of 200 were selected for the interactive evaluation. The MDCT angiographic data were analysed independently by three radiologists for the Study IV. The observers first viewed the bifurcation area of both carotids interactively at the workstation to obtain a general overview of the vessels and to detect the possible sites of stenosis and additional findings. Filling pouch of contrast media within the plaque was interpreted as ulceration.

The distal cervical and intracranial parts of the ICA were evaluated by one of the observers in the cine mode in three orthogonal planes for detection of significant distal stenosis above bifurcation as a possible tandem lesion and also for detection of other findings.

4.2.8.2. Measurements

4.2.8.2.1 SDCT angiography (Study II)

The corresponding axial levels of CT angiography and 3D TOF MRA source images were identified on the basis of the distance from the position of the flow divider. Measurements were done from a total of 45 axial images with IVUS as a reference. One radiologist measured the CT angiography images twice with an interval of two months between measurements. Measurements were also performed from 9 axial slices corresponding to the levels of histological specimens, and so altogether 54 levels were reviewed for the analysis of CT angiography measurement reproducibility and for the comparison of CT angiography and 3D TOF MRA measurements.

For the assessment of the degree of stenosis, the smallest bisecting luminal diameter at the most severe stenosis and the reference diameter at the same site from the outer edge of the arterial wall were measured on axial images of 3D TOF MR and CT angiography. Luminal diameters and thickness of the plaque were measured from CT angiography and MRA axial source images.

On contrast angiography, the diameter stenosis degree was measured according to the European Carotid Surgery Trial criteria (230), analogous to the axial IVUS, CT angiography and 3D TOF MRA measurements. For CT angiography and 3D TOF MRA source images and for contrast angiography, measurements were performed with a digital micrometer on a film viewer at approximately threefold magnification.

4.2.8.2.2 MDCT angiography (Studies III-IV)

For the Study III, the automated 3D CTA analysis program was used to assess the degree of stenosis of both carotid arteries. The program assessed the cross-section area of the artery lumen based on density and reconstructed a three-dimensional image. After selection of the level of reference and the lower and upper margins of the stenosis on the lumen image, the workstation automatically assesses the level of maximal stenosis.

The image quality and all misregistrations of the enhanced carotid artery lumen boundaries by the 3D CTA analysis method were registered by one observer, who performed the first measurements without any corrections of the misregistrations of the automated analysis program. Two months after the first measurements, one observer performed the measurements for the second time, and manual corrections were now applied to correct for the errors of the delineation of the vessel lumen by

the 3D CTA analysis method. The second observer performed the measurements with the 3D CTA analysis method using manual corrections if needed.

Detailed diameter measurement values given by the program were registered by two observers both at the site of the maximal stenosis and at the site of the reference level in the ICA distal to the carotid bulb. The percentages of 0–29, 30–49, 50–69, 70–99, and 100 were used to categorise the degree of stenosis.

For the assessment of the degree of stenosis in the Study IV, the oblique cross-sectional MPR (cMPR) and oblique sagittal MPR (sMPR), which are perpendicular to each other, were reconstructed by each observer. Two observers independently measured the diameter stenosis degree using the NASCET criteria. The measurements were performed from magnified MPR images with an electronic caliber at the workstation. To assess intraobserver repeatability, one observer without previous experience of performing CT angiography analysed the data twice with an interval of one month.

4.2.9. Statistical methods

The measured degrees of stenosis expressed as continuous variables were tested for normal distribution by the Kolmogorov-Smirnov 1-sample test. Differences for continuous variables with a normal distribution were analysed with Student's *t*-test for paired observations. A p value of less than 0.05 was considered to indicate a statistically significant difference. In the Study I, due to an unacceptable bias from normality, the Wilcoxon matched-pairs signed-ranks test was used to compare the diameter stenoses measured by the two imaging modalities.

The Pearson correlation coefficient was calculated to assess the intraobserver reproducibility and the interobserver/intertechnique agreement. The kappa statistic

(κ) was used to calculate the intra- and interobserver agreement of the dichotomised values of the visual grading and measurements of the degree of stenosis. A κ coefficient greater than 0.75 represented excellent agreements, 0.40 to 0.75 fair to good agreement, and less than 0.40 poor agreement (231).

The sensitivity, specificity and overall accuracy (diagnostic performance) of CT angiography (Studies I-IV) and 3D TOF MRA (II study) were calculated using dichotomised values of the degree of stenosis and for the detection of atherosclerotic lesion and plaque calcification (Study II). In addition, the diagnostic performance of carotid MDCT angiography with positive and negative predictive values was calculated separately for the symptomatic side.

In the Study II, the consistency between readers in the detection of plaque calcification is given as percent agreement. In addition, mean difference with SD was calculated for the intra- and interobserver agreement of measurements and for the intertechnique comparison. Table 6 shows the summary of the statistical methods of the study.

The data were analysed with the SPSS/PC+ 5.01 and with the SPSS 11.5 for Windows (SPSS Inc. Chicago, IL, USA) statistical packages.

Table 6. Summary of the statistical methods of the study

Type of variable	Purpose	Test	Significance	Study
Continuous variable	Test for the distribution of values	Kolmogorov-Smirnov 1-sample test	$p < 0.05$	I-IV
Paired continuous variables with normal distribution	Interobserver reproducibility Intertechnique variability	Student's *t*-test	$p < 0.05$	II-IV
Paired continuous variables with non-normal distribution	Intertechnique variability	Wilcoxon matched-pairs signed-ranks test	$p < 0.05$	I
Paired continuous variables	Intraobserver reproducibility Interobserver variability Intertechnique variability	Pearson correlation	$p < 0.05$	II-IV
Categorical variable (dichotomised values of the stenosis grading)	Intraobserver agreement Intertechnique agreement	kappa (κ)	Agreement: < 0.40 poor 0.40 - 0.75 fair to good > 0.75 excellent	I,II,IV
Categorical variable (dichotomised values of the stenosis grading)	Diagnostic performance of the imaging method	Sensitivity Specificity Overall accuracy Positive predictive value (PPV) Negative predictive value (NPV)		I-IV I-IV I-IV IV IV
Categorical variable	Interobserver agreement Intertechnique agreement	Percent agreement		II-IV

5. RESULTS

5.1. ASSESSMENT OF RENAL ARTERY STENOSIS (Study I)

5.1.1. DSA and CT angiography findings

Two renal arteries each had two separate calcified lesions; these were interpreted as separate stenosed segments. Therefore, a total of 80 renal artery segments were evaluated. According to DSA, 55 segments were grade I, 20 grade II and 4 grade III stenoses. Among the 55 grade I segments, 27 were minimally stenosed (< 30%) or normal. One mild segmental branch stenosis detected by DSA was also evident in CT angiography. Evaluated from the MIP images, 33 segments were noncalcified, 11 had mild calcification and 36 were heavily calcified. Thus, the proportion of calcified lesions was 59%.

5.1.2. Intraobserver reproducibility and interobserver agreement

The intraobserver repeatability was good to excellent for reading both the MIP images (k=0.72, 95% confidence interval 0.57,0.88) and the combined MIP+MPR images (k=0.76, 95% confidence interval 0.62,0.91) The kappa statistic for interobserver consistency of interpretation of the MIP images was 0.60 (95% confidence interval 0.42,0.79) and for the combined MIP/MPR images 0.44 (95% confidence interval 0.27,0.62).

5.1.3. Visual interpretation

Both observers reached 100% sensitivity for the MIP film reading, with a specificity of 42%-54%. By combining the MIP+MPR readings, specificity values increased to 58%-84%, but the rate of false negatives increased 4%-16%. The corresponding

values for sensitivity, specificity and overall accuracy calculated separately for the subgroups of calcified and noncalcified lesions are given in Table 7, which shows that the diagnostic performance of visual CT angiography interpretation is clearly less accurate for calcified lesions. While the combined MIP+MPR image reading method improved specificity in both groups, this resulted in deterioration of sensitivity for calcified lesions.

Table 7. Sensitivity, specificity and overall accuracy for the subgroups of calcified and noncalcified renal artery segments

Calcified renal artery segments (n=47)				
Observer	Reconstruction	Sensitivity	Specificity	Accuracy
1	MIP	100 (17/17)	31 (9/30)	57 (26/47)
	MIP/MPR	77 (13/17)	70 (21/30)	72 (34/47)
2	MIP	100 (17/17)	27 (8/30)	53 (25/47)
	MIP/MPR	94 (16/17)	37 (11/30)	58 (27/47)
Noncalcified renal artery segments (n=33)				
1	MIP	100 (8/8)	80 (20/25)	85 (28/33)
	MIP/MPR	100 (8/8)	100 (25/25)	100 (33/33)
2	MIP	100 (8/8)	60 (15/25)	70 (23/33)
	MIP/MPR	100 (8/8)	84 (21/25)	88 (29/33)

Note –MIP, maximum intensity projection; MPR, multiplanar reformation

5.1.4. Quantitative measurements

The mean percent diameter stenosis as measured from the MIP images (49%, range 0-85) was statistically significantly (p<0.001) higher than that from the DSA films (mean 35%, range 0-87). Stenosis degrees measured from the MPR images (mean 41%, range 0-83) were closer to the DSA measurements (p=0.709). Sensitivity, specificity and overall accuracy values for the MIP measurements were 96%, 62%, and 73% and for the MPR measurements 72%, 80%, and 78%, respectively, for detection of haemodynamically significant stenosis. Because of the

systematic overestimation of the MIP measurements compared to DSA, the sensitivity, specificity and overall accuracy values were also calculated using 60% diameter stenosis as a cut off point for significant stenosis by MIP. This improved the diagnostic performance, yielding sensitivity, specificity and overall accuracy values of 92%, 76%, and 81%.

5.1.5. Visual interpretation combined with quantitative measurements

In an attempt to improve the poor specificity of MIP film reading, quantitative stenosis measurements were made as an adjunct to the visual reading. In this interactive analysis method, the MIP images were first interpreted visually, and then those stenoses interpreted as haemodynamically significant were measured from the MIP images. Only those stenoses exceeding 60% in the quantitative measurements were classified as significant. This diagnostic algorithm performed as visual interpretation of MIP images combined with quantitative measurements using ≥60% as the cutoff point of significance yielded sensitivity, specificity and overall accuracy values of 92%, 80%, and 84%, respectively for both observers. Figure 3 shows the diagnostic accuracy of SDCT angiography with various algorithms to assess RAS.

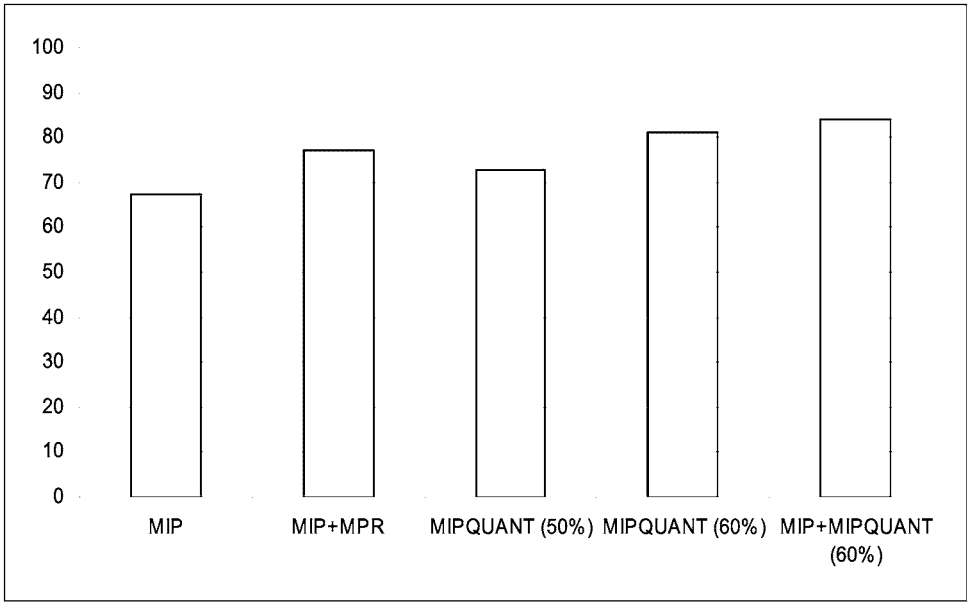

Figure 3.

The overall accuracy of various diagnostic algorithms of single-detector CT angiography for detecting haemodynamically significant renal artery stenosis. Results of the two observers are averaged.
MIP, visual interpretation of the maximum intensity projection (MIP) images
MIP+MPR, visual interpretation of the MIP and multiplanar reformation (MPR) images together
MIPQUANT (50%), measurement of the degree of stenosis from the MIP films in percentages using ≥ 50% as the cutoff point for significance
MIPQUANT (60%), measurement of the degree of stenosis from the MIP films in percentages using ≥ 60% as the cutoff point for significance
MIP+MIPQUANT (60%), visual interpretation of the MIP images combined with measurement of the degree of stenosis from MIP films using ≥ 60% as the cutoff point for significance

5.1.6. Renal cortical enhancement measurements

Eight of the 26 patients included in this analysis had a ≥ 50% difference in the diameter stenoses between the right and left kidney in DSA. The ratios of the

enhancement values of the kidneys in CT ranged from 0.93 to 1.18 (mean 1.01). The cut-off points <0.95 or >1.05 for the ratio of enhancement values between the right and left kidneys were 84% sensitive, 71% specific and had an overall accuracy of 81% for diagnosing a difference of 50% or greater in percent diameter stenoses of the renal arteries.

5.2. CAROTID ATHEROSCLEROSIS DETECTION WITH SDCT ANGIOGRAPHY IN COMPARISON TO 3D TOF MRA (Study II)

5.2.1. Image quality

A total of 21 patients underwent both CT angiography and 3D TOF MRA. This study population was used for the analysis of image quality and visual interpretation consistency. Altogether 168 carotid segments were analysed, but 19 were excluded because of a limited scan volume of CT angiography and 3D TOF MRA. In these 19, the distal carotid artery was not properly included in the imaging volume of either modality. Thus, a total of 149 segments were included for the comparative analysis. The quality of CT angiography was assessed as good in 46% and 52%, satisfactory in 42% and 52%, and poor in 2% and 6% of the segments by the two readers.

The poor quality of CT angiography images was mainly due to poor differentiation of the vessel wall from the surrounding structures or poor arterial contrast medium enhancement predominantly in distal parts of the imaging volume.

On 3D TOF MRA the quality of the images was assessed as good in 17% and 43%, satisfactory in 39% and 70%, and poor in 13% and 18% of the analysed segments. The poor quality of some 3D TOF MRA images was mainly caused by signal loss in slices located at the periphery of the imaging slab, and sometimes also by motion artefacts or turbulent flow.

5.2.2. Reproducibility and interobserver agreement

The interobserver agreement for the detection of atherosclerotic lesions by CT angiography was good (κ=0.56, 95% confidence interval 0.40-0.72). The interobserver agreement for visual estimation of diameter stenosis degree exceeding 50% was excellent with CT angiography (κ=0.83, 95% confidence interval 0.71-0.94) and fair with 3D TOF MRA (κ=0.47, 95% CI 0.29-0.66). The interobserver agreement for the detection of plaque calcification by CT angiography was excellent; the overall agreement was 94% for the two readers. In 3D TOF MRA the two readers agreed in 73% of the analysed segments for the presence of calcifications. The intraobserver reproducibility of various measurements from CT angiography images was good; the Pearson correlation coefficient for repeated diameter stenosis measurements was 0.85 (p<0.001, n=54), for luminal diameter measurements 0.87 (p<0.001, n=54) and for measurements of plaque thickness 0.83 (p<0.001, n=54).

5.2.3. Detection of atherosclerotic lesions

Contrast angiography revealed altogether 51 stenotic lesions in the 55 arteries. None of the stenotic lesions detected in contrast angiography was missed on CT or 3D TOF MRA axial source images. Atherosclerotic lesions were detected by CT angiography bilaterally in one patient, whereas contrast angiography was normal. Nineteen percentages of the evaluated carotid segments with atherosclerosis in CT angiography were normal in contrast angiography.

IVUS revealed a total of 29 atherosclerotic lesions on the ten carotid arteries, all with a stenosis of less than or equal to 40%, and 16 of which were not seen on contrast angiography. The diagnostic performance of CT and 3D TOF MRA for

plaque detection from axial source images with IVUS as a reference was moderate to good for the two observers, with an overall accuracy varied between 64 and 80%.

With reference to consensus reading performed by readers 1 and 2 for detection of plaque calcifications on CT angiography, the overall accuracy of 3D TOF MRA was 79% and 72% for the two readers with a sensitivity of 53% and 61% and specificity of 87% and 74%.

Plaque ulceration was seen on contrast angiography in eight arteries of six patients. On CT angiography one ulcer was detected by both readers, and two other ulcers were suspected by one reader. Further, 3D TOF MRA was performed on three of the patients with ulcers on contrast angiography, and two of these patients had ulcers in both left and right carotids. None of these five ulcers were detected in 3D TOF MRA axial source images by either of the two readers.

5.2.4. Quantitative measurements

5.2.4.1. Diameter stenosis

The mean diameter stenoses for contrast angiography, CT angiography and 3D TOF MRA were 24% (range 4 - 74%), 42% (range 20 - 87%) and 59% (range 7 - 100%) for the 54 levels that were analysed. The Pearson correlation coefficient for diameter stenosis degree measurements was 0.71 ($p < 0.001$) between contrast angiography and CT angiography, and 0.75 ($p < 0.001$) between contrast angiography and 3D TOF MRA.

Table 8 presents the accuracy of CT angiography and 3D TOF MRA in the assessment of diameter stenosis degree using IVUS as a standard of reference. The large number of false positive findings on CT angiography with a cutoff point $\leq 20\%$ between normal and abnormal findings was mainly caused by large calcifications.

Both CT angiography and 3D TOF MRA missed four stenotic lesions with a cutoff point ≤ 10% between normal and abnormal finding, and the maximum degree of stenosis (15% and 16%) among the false negatives did not differ significantly between the modalities.

Table 8. The diagnostic performance of CT and MR angiography (axial source images) measurements with reference to intravascular ultrasound, (n=45) using various diameter stenosis values as cutoff points between normal and abnormal findings

Cut-off point	Sensitivity%	Specificity%	Overall accuracy%
≤ 10% vs > 10%			
CT angiography	96	64	80
MR angiography	87	46	67
≤ 20% vs > 20%			
CT angiography	100	43	53
MR angiography	100	73	78

The diameter stenosis measurements from 45 axial slices varied between 0-60% (mean 24%) on CT angiography, 0-40% (mean 17%) on 3D TOF MRA and 0-40% (mean 11%) on IVUS. Measurements of diameter stenosis (n=45) from CT angiography correlated slightly better with those from IVUS (r=0.77, p<0.001) than did those from 3D TOF MRA (r=0.53, p<0.001).

One weakness of 3D TOF MRA was the large number of false positive findings, mainly caused by turbulent flow after a tight stenosis or by slow flow phenomena such as flow separation and vortex flow. CT angiography suffered from the poor distinction of vessel wall from surrounding structures. This phenomenon interfered with the detection of atherosclerosis in some carotid artery segments.

5.2.4.2. Luminal diameters and plaque thickness

On CT angiography, the measurements of luminal diameters (n=45) at the site of tightest stenosis correlated closely with the corresponding measurements on IVUS ($r = 0.73$, $p < 0.001$), and the measurements of plaque thickness (n=45) also correlated well ($r = 0.72$, $p < 0.001$). For 3D TOF MRA, the correlation of the luminal diameter ($r = 0.85$, $p < 0.001$) and plaque thickness ($r = 0.48$, $p < 0.001$) measurements (n = 45) with those of IVUS were also statistically significant. The mean difference of the luminal diameters at the site of tightest stenosis was 1.1 ± 0.8 mm (± standard deviation, SD) between CT angiography and IVUS, and 0.7 ± 0.7 mm (± SD) between 3D TOF MRA and IVUS. The mean difference for plaque thickness was 1.2 ± 1.1 mm (± SD) between CT angiography and IVUS, and 0.7 ± 0.7 mm (± SD) between 3D TOF MRA and IVUS.

5.3. ASSESSMENT OF CAROTID STENOSIS WITH MDCT ANGIOGRAPHY IN SYMPTOMATIC PATIENTS (Studies III-IV)

5.3.1. The quality of carotid MDCT angiography

5.3.1.1. Image quality

All images of CT angiography in the 72 carotids were diagnostic, with 67 images of good quality. The image quality of five vessels was suboptimal, but still diagnostic. The poorer quality was due to high densities caused by high enhancement in the adjacent jugular vein (n=2), a low intraluminal low enhancement in both carotid arteries (n=2), or a motion artifact (n=1) at the bifurcation of one carotid artery. The motion artifact was avoided on the other side by the higher location of the contralateral carotid bifurcation.

5.3.1.2. Quality of the 3D CTA automated analysis method

There were several misregistrations of the enhanced carotid artery lumen by the 3D CTA automated analysis method. An interfering factor was registered in 27 arteries at the level of the stenosis, and in 6 cases at the reference level. Intramural calcifications were found to be the most common interfering factors leading to the misregistration of the borders of contrast enhanced lumen in the carotid bifurcations. There were 14 (42%) calcifications and 5 (15%) ulcerations at the level of measurements. The other interfering factors included bifurcating vessels (n=2), adjacent bypassing vessels (n=2), partial-volume effects from short segment stenosis (n=2), and intraluminal low contrast media density (n=4).

5.3.2. Reproducibility analysis

5.3.2.1. 3D CTA automated analysis

Altogether 12 of 72 carotid arteries changed from their original stenosis category in the five-point grading scale to another stenosis category after manual correction of the misregistration in the 3D CTA automated analysis. However, only one stenosis changed across the 70% cut-off point. In the comparison between the two manually corrected 3D CTA automated analysis measurements by the same radiologist, 49 (68%) of the 72 vessels exactly agreed with each other according to NASCET categories. The mean difference between those repeated measurements of the degree of stenosis was 4.06% with standard deviation of 29.6%. The intraobserver correlation coefficient was 0.89.

The mean difference between the measurements of the two observers was 0.37 with standard deviation of 33.0. The interobserver correlation coefficient was 0.90.

5.3.2.2. MPR measurements

The interobserver correlation coefficient between the repeated stenosis degree measurements (n=70) was 0.79 ($p < 0.001$) using cMPR and 0.77 ($p < 0.001$) using sMPR. The interobserver correlation coefficient was 0.83 ($p < 0.001$) for the cMPR measurements and 0.77 ($p < 0.001$) for the sMPR measurements.

Fair to moderate agreement was found between the two observers at the cut-off point of 50% stenosis degree, achieving a kappa statistic value of 0.52 (95% confidence interval; 0.32 - 0.72) for cMPR and 0.49 (0.30 - 0.69) for sMPR.

5.3.3. Diagnostic performance of carotid MDCT angiography measurements

5.3.3.1. 3D CTA automated analysis

Diagnostic performance by sensitivity, specificity, and overall accuracy for 3D CTA automated analysis with reference to conventional DSA (n=72) were 52% (12/23), 94% (46/49), and 81% (58/72), when using the cut-off point of 70% or more for the significant finding. The corresponding values of diagnostic performance for manually corrected 3D CTA automated analysis were almost similar: 47% (11/23), 94% (46/49), and 79% (57/72), respectively.

5.3.3.2. MPR measurements

The correlation coefficient between CT angiography and rotational angiography measurements of the smallest diameter of the absolute residual lumen of carotid stenosis was 0.75 ($p < 0.001$) using cMPR and 0.66 ($p < 0.001$) using sMPR for the first measurer and the corresponding values for the second measurer were 0.84 ($p < 0.001$) and 0.83 ($p < 0.001$). The accuracy of CT angiography in the measurement of degree of stenosis in the carotid bifurcation area with reference to rotational

angiography is shown in Table 9. Table 10 shows the diagnostic performance of CT angiography measurements in comparison with DSA. The combined MPR was considered to be positive when either the cMPR or sMPR measurements yielded a degree of stenosis ≥ 50%.

TABLE 9. CT angiography MPR measurements of the degree of stenosis in carotid arteries compared with rotational angiography *(n=33)*

MPR measurement method	Observer	Mean difference % ± SD	r	κ (95% CI) 50%*	κ (95% CI) 70% †
Cross-sectional MPR	1	6.9 ± 17.6	0.82	0.58 (0.31-0.84)	0.40 (0.05-0.76)
	2	10.7 ± 16.1	0.86	0.58 (0.33-0.83)	0.29 (-0.04-0.62)
Sagittal MPR	1	2.8 ± 19.2	0.80	0.70 (0.45-0.94)	0.40 (0.05-0.76)
	2	9.1 ± 16.8	0.84	0.58 (0.31-0.84)	0.42 (0.06-0.76)

Note — MPR, multiplanar reformation; r, Pearson correlation coefficient; κ, kappa statistics; CI, confidence interval
*50% cut-off point for significant stenosis
†70% cut-off point for significant stenosis
A positive mean difference value in the table indicates an underestimation of the degree of stenosis with CT angiography

TABLE 10. Diagnostic performance of various CT angiography analysis methods in the assessment of the degree of stenosis in carotid arteries *(n=70)* in comparison with DSA using 50% stenosis as the cut-off point for a significant finding

Analysis Method of CT angiography	Observer	Sensitivity % (n/n)	Specificity % (n/n)	Overall accuracy % (n/n)
Cross-sectional MPR	1	73 (22/30)	80 (32/40)	77 (54/70)
	2	77 (23/30)	98 (39/40)	88 (62/70)
Sagittal MPR	1	87 (26/30)	70 (28/40)	77 (54/70)
	2	87 (26/30)	95 (38/40)	91 (65/70)
Combined MPR	1	87 (26/30)	70 (28/40)	77 (54/70)
	2	90 (27/30)	95 (38/40)	93 (66/70)

Note — DSA, digital subtraction angiography; MPR, multiplanar reformation
The combined MPR was considered to be positive when either of the MPR (cross-sectional or oblique sagittal) measurements yielded a positive result

5.3.4. Diagnostic performance of visual estimation and interactive interpretation

5.3.4.1 Visual estimation

Simple visual estimation of the degree of stenosis yielded sensitivity of 100% (31/31), specificity of 73% (29/40) and overall accuracy of 86% (60/70) when using DSA as the standard of reference.

5.3.4.2. Interactive interpretation

An additional strategy was tested using the highly sensitive visual estimation as the first line screening step for the detection of a significant stenosis (≥ 50%), and as the second step, the measurement of the degree of stenosis was applied only for the positive cases selected by visual estimation i.e. interactive interpretation was used. In symptomatic sides (n=35), the sensitivity of CT angiography was good with sufficient accuracy for the detection of carotid stenosis (Table 11). The only false positive case with CT angiography was a carotid bifurcation with the stenosis degree of 62% on cMPR and 59% on sMPR, in which the stenosis degree was measured to be 43% on DSA, but 63% on rotational angiography.

CT angiography detected 14 ulcerative plaques in the 65 patent carotid arteries. In eleven cases the finding agreed with DSA. Fourteen of the ulcerations diagnosed on DSA were not detected on CT angiography. Therefore, the agreement between CT angiography and DSA was 74% for the detection of plaque ulceration.

All five occlusions in proximal ICAs verified with DSA were correctly diagnosed on CT angiography by all observers. In the remaining 66 patent ICAs, distal lesions were interpreted to be present in 13 (20%) cases with CT angiography. Four false positive findings were due to the presence of extensive calcifications. Since there were no

false negative findings on CT angiography, sensitivity of 100% (9/9), specificity of 93% (53/57), and overall accuracy of 95% (62/65) was achieved for the detection of distal lesions in the ICA. The one incidental middle cerebral artery aneurysm was correctly diagnosed by CT angiography.

TABLE 11. Diagnostic performance of CT angiography in the assessment of carotid artery stenosis on symptomatic side *(n=35)* compared with DSA using 50% stenosis as the cut-off point for a significant stenosis

Analysis Method of CT Angiography	Sensitivity % (n/n)	Specificity % (n/n)	Overall accuracy % (n/n)	PPV % (n/n)	NPV % (n/n)
Visual	100 (21/21)	50 (7/14)	80 (28/35)	75 (21/28)	100 (7/7)
Combined MPR	95 (20/21)	86 (12/14)	91 (32/35)	91 (20/22)	92 (12/13)
Visual-Quantitative analysis	95 (20/21)	93 (13/14)	94 (33/35)	95 (20/21)	93 (13/14)

Note — DSA, digital subtraction angiography; MPR, multiplanar reformation; PPV, positive predictive value; NPV, negative predictive value
The combined MPR was considered to be positive when either of the MPR (cross-sectional or oblique sagittal) measurements yielded positive result
Visual-quantitative analysis consisted of first-line visual CT angiography interpretation and subsequent measurement only for the positive cases

6. DISCUSSION

Atherosclerotic disease in renal and carotid arteries has a considerable clinical significance due to its serious complications. Angiography is still the gold standard for the final diagnostic purposes before the treatment of symptomatic disease. However, due to risks associated to invasive angiography, alternative imaging methods have been developed for the screening of renal artery stenosis and carotid artery atherosclerotic disease. Surgical treatment has been considered to be effective for the prevention of the complications of atherosclerotic disease. Endovascular interventions have offered an alternative choice for the treatment of atherosclerotic lesions in arteries. The use of noninvasive imaging methods helps in the selection of appropriate treatment in each case. The treatment decision relies often on a single measurement of the degree of stenosis. This study focuses in the imaging of renal and carotid arteries with CT angiography mainly for clinical diagnostic purposes.

6.1. SDCT ANGIOGRAPHY OF RENAL ARTERIES (Study I)

Visual reading of MIP films yielded sensitivity of 100% but only 42-55% specificity for the detection of renal artery stenosis (Study I). Our results are comparable with those reported by Rubin et al. (70) (sensitivity 92% and specificity 83% for the detection of $\geq$ 70% stenosis with MIP), although the proportion of calcified lesions in that study was smaller than ours (29% vs. 59%). Beregi et al (112) used the same collimation and pitch in their study for screening hypertensive patients (n=50) as we had in our study. They reached 100% sensitivity when their material was analysed by excluding accessory arteries and 88% sensitivity when two accessory arteries were included. When screening the hypertensive population, the proportion of calcified

lesions might be smaller than that seen among these patients suffering mostly from disorders of advanced atherosclerosis.

The MIP film reading resulted in numerous false positive findings, especially when the lesion was calcified, a result reported also by others (70). We therefore analysed the value of MPR films as an adjunct to the MIP images. This strategy improved the specificity for interpreting calcified lesions from 27% - 31% to 37% - 70% for the two observers. A decrease in false positive results was achieved at the expense of a small increase (4% - 16%) in the false negative results, however. This decrease in sensitivity invalidates the use of this diagnostic algorithm as a screening method.

We observed a systematic overestimation of the degree of stenosis as measured from the MIP films. The diagnostic performance of quantitative stenosis measurements from the MIP films, dichotomised as haemodynamically significant stenoses versus nonsignificant lesions, was not clearly better than that obtained by visual assessment (overall accuracy of 73% versus 60% - 75%). Although stenosis quantitation from the MPR films resulted in a somewhat better specificity than the MIP measurements (80% vs. 62%), the 28% rate of false negative findings is far from acceptable for a diagnostic screening method. The selection of 60% diameter stenosis as a cutoff point for significant stenosis from the MIP films resulted in a somewhat better diagnostic performance, but still suffered from a 24% rate of false positive findings. The best results were obtained from the combined use of visual reading of the MIP films plus quantitative measurements of those stenoses interpreted as haemodynamically significant. By grading only those stenoses exceeding 60% in quantitative measurements as haemodynamically significant, the rate of false positive findings decreased to 20% with only a modest decrease in sensitivity.

The usefulness of estimation of renal cortical enhancement visually (70) or with measurements (63) has been dealt with in recent studies. High specificity in depicting > 70% stenosis was achieved when abnormal nephrograms were observed visually from the MIP or SSD reconstructions (70), and the result of another study employing measurements seems to be similar (63). We measured the cortical enhancement values at the center of the imaging volume and calculated the ratio between the kidneys. Although this technique revealed unilateral haemodynamically significant stenoses with reasonable accuracy, it is cumbersome and unsuitable for the evaluation of kidneys with multiple renal arteries or bilateral significant renal artery stenosis.

The screening of RAS in patients suspected renovascular hypertension before angiography is under discussion. Due to the limitations and higher cost of MRA, the use of CD-US and scintigraphy as the primary studies in screening of renovascular hypertension has been proposed (232). Based on the meta-analysis of original studies validating the accuracy of CT angiography, MRA with and without a contrast agent, US, captopril scintigraphy and the captopril test for the screening of renovascular hypertension it seems that CT angiography and MRA with a contrast agent have the highest diagnostic performance for RAS screening (233). In that meta-analysis, non-enhanced MRA, CD-US and captopril scintigraphy were better than the captopril test. However, in a multicenter study evaluating only patients with the suspicion of renovascular mechanism for hypertension, the sensitivity of both CT angiography and contrast-enhanced MRA was low; 64% and 62%, respectively (234). In additional analyses of this multicenter study among patients with advanced age, organ damage and atherosclerotic renal artery disease the sensitivity of CT angiography and contrast-enhanced MRA was higher, but according to the authors

sensitivity of these methods is not high enough to justify their use for RAS screening (234). The accuracy of CT angiography and MRA for the detection of fibromuscular dysplasia in renal arteries was poor. While technical developments of CT and MR devices allows imaging of renal arteries with higher resolution (118, 235), further studies are warranted to evaluate the role of CT angiography and contrast-enhanced MRA in the screening of renovascular hypertension. There are no updated international quidelines for the imaging strategies for the screening of renovascular hypertension. An electronic article (http://www.emedicine.com/med/topic2006.htm) by experts in renovascular hypertension recommends screening with CT angiography, MRA or US according to the availability of these studies and local experience. DSA is still the 'gold standard' validating the positive findings of screening studies. After a positive finding in a screening study, DSA is usually performed before endovascular intervention.

6.2. SDCT ANGIOGRAPHY FOR THE DETECTION OF CAROTID ATHEROSCLEROSIS (Study II)

As a consequence of the inclusion criteria (in connection with neurointerventional procedures) used for the patients undergoing the IVUS examination in this study, the mean diameter stenosis degree on IVUS was low (mean 35%, range 4-40%). This allowed verification of the diagnostic performance of CT angiography and 3D TOF MRA in detecting minor atherosclerotic lesions of carotid arteries. The repeatability of CT angiography for the measurements of lumen diameter, plaque thickness and diameter stenosis from the axial source images was excellent. Even for subtle stenoses, the sensitivity of SDCT angiography was excellent (96% - 100%) when IVUS was used as a reference. Intraplaque calcifications and anatomic vascular

structures facilitate the precise localisation and identification of atherosclerotic plaque as a target for measurements, even between successive studies. Based on the results of the present study, CT angiography seems to be an adequate follow-up imaging method for the aims of prospective studies.

CT angiography depicted all stenotic lesions of the carotid arteries evident in contrast angiography. Moreover, CT angiography also detected concentric stenoses not detectable in contrast angiography. The difference between contrast angiography and CT angiography diameter stenosis measurements may be even greater because of the inability of contrast angiography to detect the compensatory arterial enlargement during the development of the atherosclerotic process (236). Furthermore, the authors of a study using rotational angiography as a reference suggested that conventional angiography with two or three projections often underestimates the degree of stenosis compared with measurements obtained with rotational angiography (182). In that study, conventional angiography often failed to show the most stenosed part of the lesion, or in the optimal projection the stenosed segment was covered by other vascular structures (182). Complex vascular anatomy does not hamper the quality of CT angiography, and the reconstructions can be created in any projection without artefacts from surrounding structures (87).

We found a reasonable correlation between various measurements from IVUS imaging and CT angiography axial source images (diameter stenosis, luminal diameter, plaque thickness). The correlation was of the same order between 3D TOF MRA and IVUS. However, somewhat better interobserver agreement was obtained in CT angiography than in 3D TOF MRA when diameter stenosis was graded visually by the readers. Furthermore, the image quality of CT angiography was more uniform.

Both CT angiography and 3D TOF MRA showed a tendency to overestimate the degree of diameter stenosis in comparison with IVUS. Most of the major overestimations of diameter stenosis degree with CT angiography occurred because of the enlargement of intraplaque calcifications by the partial volume effect. This phenomenon is a disadvantage of CT angiography when precisely assessing the diameter stenosis, but it is not particularly problematic in follow-up.

The detection of calcification is valuable for the estimation of the thromboembolic predisposition of the carotid atherosclerotic lesion, since plaque calcifications are thought to be associated with more stable plaques. Previously it has been established that IVUS reliably detects macroscopic calcifications of plaques in carotid arteries with reference to histopathologic findings, whereas punctate calcifications are missed (221). Without histopathologic verification the diagnostic accuracy of CT angiography for the detection of punctate calcifications remains unknown. For the detection of calcification, 3D TOF MRA proved to be less sensitive.

6.3. CAROTID MDCT ANGIOGRAPHY IN SYMPTOMATIC PATIENTS (Studies III-IV)

Irregular eccentric stenoses with a noncircular lumen are common in carotid arteries. Therefore, the shortest diameter of stenosed carotid segment is more likely revealed accurately with rotational angiography producing more projections than DSA. In our study the measurements from DSA tended to give slightly smaller degrees of stenosis than rotational angiography (Study IV).

Using rotational angiography as a standard of reference, the measurement of the carotid artery luminal diameter by CT angiography using MPR images was quite accurate in normal arteries and in mildly or moderately stenosed segments, but the

accuracy decreased in cases of high-grade stenosis with a very small minimal diameter of the stenosed lumen. There was considerable variability between the observers in performing the measurements in CT angiography, and the intraobserver reproducibility was not high either, probably due to the inexperience of one of the observers in interpreting CT angiography studies. Our study indicates that good experience of the radiologist interpreting CT angiography studies is essential.

There are several possible reasons for the inaccurate determination of the diameter in the carotid artery with a high-grade stenosis. One reason may be the inability of the observer to place the digital calipers accurately in a stenosed artery with very small diameter, where the caliper almost hides the vessel. When magnifying the displayed image, some blurring of the structures occurs. In addition, in our CT angiography interpretation we used a wide window and level settings in order to visualise mural calcifications properly. The study by Liu et al (237) with a vessel phantom showed that the application of optimised window and level settings on CT angiography can reduce the measurement variability, because suboptimal window and level settings are the reason for edge blurring of the enhanced vessel. The smaller the actual luminal diameter, the greater the potential measurement error. This phenomenon may partly explain the failing of CT angiography measurement to assess accurately the diameter in cases of high-grade stenoses.

In another phantom study, the reconstruction kernel for axial slices and insufficient contrast density has been proposed to be possible sources of errors for the contrast column diameter assessment with automated software (238). The movement of pulsating carotid artery during CT angiography may also cause blurring of the vessel edges and even obscure high-grade stenosis in CT angiography.

However, if it is obvious that the measured stenosis degree is not reasonably precise, as evident in our study, it is not reasonable to base the diagnosis only on a single measurement of the degree of carotid stenosis.

Conventional angiography is currently the only widely used reference method in clinical studies. In previous studies on the accuracy of CT angiography, DSA has been used as the reference. To be able to compare results with other studies for diagnostic accuracy of CT angiography, we also used DSA as a reference (Study IV). Rotational angiography has not been used in large randomised studies as a standard, and in our study rotational angiography was not always performed on the symptomatic side to get a wide range of stenosis degrees and to avoid the additional risks of angiography.

Although measurements of the absolute diameter by CT angiography were inaccurate compared with rotational angiography especially in cases of high-grade stenosis, the diagnostic performance of CT angiography using DSA as a standard of reference proved to be good (Table 10).

During the interpretation of CT angiography, it was obvious for the observers that the actual stenosis was often more severe than the numerical value of the MPR measurement. Perhaps further studies will give information on the optimal display of CT angiography to accurately measure the degree of carotid stenosis. Until then, we recommend that the visual estimation of the stenosis be included for the diagnosis. In addition to the interpretation based on absolute diameter measurements, a third radiologists visually interpreted CT angiography using interactive interpretation of axial slices and MPR views for the diagnosis and simply estimated the degree of stenosis. Visual estimation proved to be the most sensitive method for identification of carotid stenosis of 50% or more, but specificity was only modest. The combination

of interactive interpretation of CT angiography with subsequent MPR measurements for selected cases achieved the best diagnostic accuracy (Table 11).

CT angiography for the symptomatic side showed a sensitivity of 95%, specificity of 93% and overall accuracy of 94%. In the study by Anderson et al (140), CT angiography with the interpretation of axial source images proved to be 89% sensitive, 91% specific and 90% accurate in the detection of carotid stenosis over 50%. Our result is comparable with that study, which was carried out with single-detector device, but in contrast, we did not have any unsuccessful CT angiography studies to exclude from the analysis. The use of bolus triggering during CT angiography ensures sufficient contrast density in target vessels. In addition, the use of high-concentration contrast media for CT angiography studies has been recommended (98). Before the scanning, training of the patient is also essential to reduce artifacts due to swallowing and moving.

For contrast-enhanced MR angiography, sensitivities as high as 100% for carotid stenosis have been reported, but spatial resolution remains poor for small vessels (239). CT angiography with multidetector-row technique has excellent spatial resolution also for smaller structures, but artefacts sometimes hamper the visualisation of short stenoses (109). Our MDCT angiography study was performed with a four-channel CT device. The capacity of newer multidetector CT devices with up to 64 slices per rotation is superior to the device used in our study. The 16-row multidetector CT device nowadays available for carotid imaging in our department produces images with fewer artifacts (Figure 2). In addition, the use of ECG-gated imaging significantly reduces the movement artifacts in CT angiography, and can be used also for carotid arteries in cases with suspicion of tight stenoses. Alternatively, in ambiguous cases the use of conventional angiography is advisable. Arguments for

the use of conventional angiography for the confirmation of high-grade stenosis in symptomatic patients have also been proposed earlier to ensure appropriate treatment decisions (206).

Ulcerative plaques in carotid arteries may be the source of thromboembolism into the cerebral circulation (240). There was moderate agreement between the modalities for the detection of ulceration in the present study. Without proper verification of the plaque (pathoanatomical diagnosis), the true accuracy of each modality remains unknown. The accuracy of CT angiography for detecting carotid artery occlusion was high in our study, in agreement with previous studies (130, 140, 241).

The sensitivity of CT angiography in this study was excellent (100%) for the detection of distal lesions in the ICA. Other clinically relevant findings may also be revealed, such as intracranial aneurysms (242).

There are also available commercial softwares for the assessment of arterial stenosis. In Study III, the automated 3D CT angiography analysis software proved to be feasible for the assessment of carotid stenosis, but the method requests manual corrections in cases of interfering factors. It should be noted that interfering factors, such as calcification, ulceration, bifurcating and bypassing vessels, short-segment stenosis, and low contrast concentration in vessel lumen often cause misregistrations of the enhanced carotid artery lumen, which should be manually corrected before the calculation of the degree of the stenosis. Most of those interfering factors causing misregistrations by the automated 3D CTA analysis program are quite easy to recognise and correct. Mural calcifications are common in atherosclerotic carotid stenoses. Mural calcifications are problematic for the assessment of the degree of stenosis with CT angiography due to the partial volume effect that enlarges the size

of the mural calcification. Mural calcification obscures the arterial lumen, leading to inaccuracies in the assessment of stenoses.

After manual corrections of the misregistrations of the 3D CTA analysis system, the reproducibility of this method was good, and the intra- and interobserver correlations were better than that of MPR measurements measured manually with electronic caliber. However, the diagnostic performance of the 3D CTA analysis method still lacks robustness.

6.4. LIMITATIONS OF THE STUDY

There are some limitations in this study. The number of the patients was small. In Study IV the small number of the patients led to a limited number of symptomatic carotid arteries, and some patients also had a normal carotid artery even on the symptomatic side. Furthermore, there were few cases with distal carotid stenosis, leading to difficulties in the interpretation of the results with regard to distal lesions. In addition, the window and level settings for the interpretation of CT angiography studies were selected empirically; but they were selected so that the mural disruptive calcifications could be well differentiated from the enhanced vessel lumen. The proper window and level settings for the display of carotid stenosis with mural calcifications is still not known, although the use of a specifically adjusted narrow window setting has been proposed (109).

The study patients were highly selected among the patients of the university hospital, and the study results cannot be transferred to any other populations. Renal artery stenosis leading to secondary renovascular hypertension is relatively uncommon. Moreover, there are also other rare diseases in renal arteries causing renovascular hypertension, which were not included in this study. The results of

Study I are therefore not universally applicable for diagnosing renal artery diseases with CT angiography in patients with renovascular hypertension. In addition, in Studies I and II film prints were used for the image analysis. In the era of digital imaging and PACS films have now disappeared, and interactive interpretation on the workstation monitor is now the only method. The interactive interpretation of CT angiography for renal arteries was not studied.

The development of CT devices has been rapid during the years when this study was carried out. A single-detector device is no longer used in our hospital. The newest CT device is a sixteen-row multidetector CT device that was not used in this study, but nowadays is in routine use for CT angiography studies. The resolution and image quality of the new MDCT devices are superior to the devices used in this study, and probably the accuracy of MDCT angiography for the imaging of atherosclerosis also is better. However, further studies are still warranted.

7. SUMMARY AND CONCLUSIONS

The purpose of this study was to evaluate the feasibility, reproducibility and accuracy of CT angiography in renal and carotid arteries. The main focus was to evaluate the diagnostic performance of CT angiography for the assessment of the degree of stenosis.

In Study I, altogether 37 patients with suspected RAS underwent SDCT angiography and the accuracy in the assessment of stenoses was assessed using DSA as a reference. Several diagnostic algorithms were studied to evaluate the usefulness of SDCT angiography for the screening of RAS. The overall accuracy of SDCT angiography with MIP film reading could be enhanced with quantitative measurement of the stenosis or reviewing the MPR images. Measuring the renal nephrograms as an adjunct to renal CT angiography provided some complementary information, but the method itself was cumbersome.

In Study II with 31 patients, DSA and IVUS were used as the references for SDCT angiography and 3D TOF MRA for the detection of atherosclerosis in carotid arteries. The carotid arteries were divided into segments for the analysis. Contrast angiography detected 51 lesions (mean diameter stenosis 50%, range 10 - 100%), and CT angiography detected the same lesions. CT angiography provided better image quality and consistency of image interpretation than 3D TOF MRA. IVUS verified 29 atherosclerotic lesions with a mean diameter stenosis of 35%, (range 4 - 40%). CT angiography yielded a sensitivity of 96% to 100% ($\leq$ 10% or $\leq$ 20% diameter stenosis regarded as normal) for the detection of lesions with reference to IVUS.

Altogether 36 consecutive, symptomatic patients underwent MDCT angiography

for Studies III and IV. The 3D CTA analysis method proved to be highly reproducible and feasible for the assessment of the degree of carotid stenosis (Study III). However, the limitations of this method must be recognised.

On the symptomatic sides (n = 35), interactive CT angiography interpretation combined with MPR measurements for lesions with a visual estimate of ≥ 50% stenosis achieved a sensitivity of 95% and specificity of 93% in the detection of carotid stenosis (≥ 50%) verified by DSA. Regardless of slight underestimation of the degree of carotid stenosis in MDCT angiography with reference to rotational DSA, the diagnostic performance of CT angiography with interactive interpretation proved to be good when using DSA as a standard of reference. MDCT angiography seems to be highly sensitive for the detection of carotid artery stenosis, suggesting the suitability of CT angiography as a screening method for symptomatic patients.

8. REFERENCES

1. Stary HC, Chandler AB, Dinsmore RE, Fuster V, Glagov S, Insull W, Jr., et al. A definition of advanced types of atherosclerotic lesions and a histological classification of atherosclerosis. A report from the Committee on Vascular Lesions of the Council on Arteriosclerosis, American Heart Association. A definition of initial, fatty streak, and intermediate lesions of atherosclerosis. A report from the Committee on Vascular Lesions of the Council on Arteriosclerosis, American Heart Association. Circulation 1995;92(5):1355-74.
2. van der Meer IM, Iglesias del Sol A, Hak AE, Bots ML, Hofman A, Witteman JC. Risk factors for progression of atherosclerosis measured at multiple sites in the arterial tree: the Rotterdam Study. Stroke 2003;34(10):2374-9.
3. von Eckardstein A, Nofer JR, Assmann G. High density lipoproteins and arteriosclerosis. Role of cholesterol efflux and reverse cholesterol transport. Arterioscler Thromb Vasc Biol 2001;21(1):13-27.
4. Tolonen H, Mahonen M, Asplund K, Rastenyte D, Kuulasmaa K, Vanuzzo D, et al. Do trends in population levels of blood pressure and other cardiovascular risk factors explain trends in stroke event rates? Comparisons of 15 populations in 9 countries within the WHO MONICA Stroke Project. World Health Organization Monitoring of Trends and Determinants in Cardiovascular Disease. Stroke 2002;33(10):2367-75.
5. Lusis AJ. Genetic factors in cardiovascular disease. 10 questions. Trends Cardiovasc Med 2003;13(8):309-16.

6. Ronnemaa T, Knip M, Lautala P, Viikari J, Uhari M, Leino A, et al. Serum insulin and other cardiovascular risk indicators in children, adolescents and young adults. Ann Med 1991;23(1):67-72.

7. Jarvisalo MJ, Raitakari M, Toikka JO, Putto-Laurila A, Rontu R, Laine S, et al. Endothelial dysfunction and increased arterial intima-media thickness in children with type 1 diabetes. Circulation 2004;109(14):1750-5.

8. Clinical reality of coronary prevention guidelines: a comparison of EUROASPIRE I and II in nine countries. EUROASPIRE I and II Group. European Action on Secondary Prevention by Intervention to Reduce Events. Lancet 2001;357(9261):995-1001.

9. Vartiainen E, Jousilahti P, Alfthan G, Sundvall J, Pietinen P, Puska P. Cardiovascular risk factor changes in Finland, 1972-1997. Int J Epidemiol 2000;29(1):49-56.

10. Tuomilehto J, Lindstrom J, Eriksson JG, Valle TT, Hamalainen H, Ilanne-Parikka P, et al. Prevention of type 2 diabetes mellitus by changes in lifestyle among subjects with impaired glucose tolerance. N Engl J Med 2001;344(18):1343-50.

11. Pentikainen MO, Oorni K, Ala-Korpela M, Kovanen PT. Modified LDL - trigger of atherosclerosis and inflammation in the arterial intima. J Intern Med 2000;247(3):359-70.

12. Berliner J, Yla-Herttuala S. The atherosclerotic lesion: a dynamic landscape. Curr Opin Lipidol 1998;9(5):385-6.

13. Johnson DE. Anatomic Aspects of Vascular Disease. In: Strandness D.E J, van Breda A. eds., editor. Vascular Diseases. New York, Edinburgh, London, madrid, Melbourne, Tokyo: Churchill Livingstone; 1994. p. 3-15.

14. Berliner JA, Navab M, Fogelman AM, Frank JS, Demer LL, Edwards PA, et al. Atherosclerosis: basic mechanisms. Oxidation, inflammation, and genetics. Circulation 1995;91(9):2488-96.

15. Nikkari ST, O'Brien KD, Ferguson M, Hatsukami T, Welgus HG, Alpers CE, et al. Interstitial collagenase (MMP-1) expression in human carotid atherosclerosis. Circulation 1995;92(6):1393-8.

16. Hunt JL, Fairman R, Mitchell ME, Carpenter JP, Golden M, Khalapyan T, et al. Bone formation in carotid plaques: a clinicopathological study. Stroke 2002;33(5):1214-9.

17. Nandalur KR, Baskurt E, Hagspiel KD, Phillips CD, Kramer CM. Calcified carotid atherosclerotic plaque is associated less with ischemic symptoms than is noncalcified plaque on MDCT. AJR Am J Roentgenol 2005;184(1):295-8.

18. Kolodgie FD, Gold HK, Burke AP, Fowler DR, Kruth HS, Weber DK, et al. Intraplaque hemorrhage and progression of coronary atheroma. N Engl J Med 2003;349(24):2316-25.

19. Kovanen P. Sepelvaltimoiden syöttösolu-allergiasolu väärässä osoitteessa? Duodecim 2004;120:126-37.

20. Knutson DW, Abt AB. Pathopfysiology, Pathology, and Clinical Features of Renovascular Hypertension. In: Jr SDE, A. vB, editors. Vascular Diseases. New York, Edinburgh, London, Madrid, Melbourne, Tokyo: Churchill Livingstone; 1994. p. 673-688.

21. Kaatee R, Beek FJ, Verschuyl EJ, vd Ven PJ, Beutler JJ, van Schaik JP, et al. Atherosclerotic renal artery stenosis: ostial or truncal? Radiology 1996;199(3):637-40.

22. Semple PF, Dominiczak AF. Detection and treatment of renovascular disease: 40 years on. J Hypertens 1994;12(7):729-34.

23. Pickering TG. Renovascular hypertension: etiology and pathophysiology. Semin Nucl Med 1989;19(2):79-88.

24. Davis SM. Extracranial and Intracranial Atheroma as Causes of Stroke. In: Myron D. Ginsberg JB, editor. Cerebrovascular Disease: Pathophysiology, Diagnosis, and Management. Malden: Blackwell Science; 1998. p. 1373-1391.

25. Hatsukami TS, Ferguson MS, Beach KW, Gordon D, Detmer P, Burns D, et al. Carotid plaque morphology and clinical events. Stroke 1997;28(1):95-100.

26. Milei J, Parodi JC, Ferreira M, Barrone A, Grana DR, Matturri L. Atherosclerotic plaque rupture and intraplaque hemorrhage do not correlate with symptoms in carotid artery stenosis. J Vasc Surg 2003;38(6):1241-7.

27. Beneficial effect of carotid endarterectomy in symptomatic patients with high-grade carotid stenosis. North American Symptomatic Carotid Endarterectomy Trial Collaborators. N Engl J Med 1991;325(7):445-53.

28. Mayberg MR, Wilson SE, Yatsu F, Weiss DG, Messina L, Hershey LA, et al. Carotid endarterectomy and prevention of cerebral ischemia in symptomatic carotid stenosis. Veterans Affairs Cooperative Studies Program 309 Trialist Group. Jama 1991;266(23):3289-94.

29. Randomised trial of endarterectomy for recently symptomatic carotid stenosis: final results of the MRC European Carotid Surgery Trial (ECST). Lancet 1998;351(9113):1379-87.

30. Rothwell PM, Eliasziw M, Gutnikov SA, Fox AJ, Taylor DW, Mayberg MR, et al. Analysis of pooled data from the randomised controlled trials of endarterectomy for symptomatic carotid stenosis. Lancet 2003;361(9352):107-16.

31. Barnett HJ, Meldrum HE, Eliasziw M. The appropriate use of carotid endarterectomy. Cmaj 2002;166(9):1169-79.

32. Risk of stroke in the distribution of an asymptomatic carotid artery. The European Carotid Surgery Trialists Collaborative Group [see comments]. Lancet 1995;345(8944):209-12.

33. Endarterectomy for asymptomatic carotid artery stenosis. Executive Committee for the Asymptomatic Carotid Atherosclerosis Study. Jama 1995;273(18):1421-8.

34. Nicolaides A, Sabetai M, Kakkos SK, Dhanjil S, Tegos T, Stevens JM, et al. The Asymptomatic Carotid Stenosis and Risk of Stroke (ACSRS) study. Aims and results of quality control. Int Angiol 2003;22(3):263-72.

35. Cherr GS, Hansen KJ, Craven TE, Edwards MS, Ligush J, Jr., Levy PJ, et al. Surgical management of atherosclerotic renovascular disease. J Vasc Surg 2002;35(2):236-45.

36. Atnip RG, Thiele BL. Surgical management of Renovascular Hypertension. In: D. Eugene Strandness Jr, Breda Av, editors. Vascular Diseases. New York: Churchill Livingstone; 1994. p. 703-720.

37. Kaukanen ET, Manninen HI, Matsi PJ, Soder HK. Brachial artery access for percutaneous renal artery interventions. Cardiovasc Intervent Radiol 1997;20(5):353-8.

38. von Knorring J, Edgren J, Lepantalo M. Long-term results of percutaneous transluminal angioplasty in renovascular hypertension. Acta Radiol 1996;37(1):36-40.

39. van de Ven PJ, Kaatee R, Beutler JJ, Beek FJ, Woittiez AJ, Buskens E, et al. Arterial stenting and balloon angioplasty in ostial atherosclerotic renovascular disease: a randomised trial. Lancet 1999;353(9149):282-6.

40. Gill KS, Fowler RC. Atherosclerotic renal arterial stenosis: clinical outcomes of stent placement for hypertension and renal failure. Radiology 2003;226(3):821-6.

41. Crowell RM, Ogilvy CS, Ojemann RG. Extracranial Carotid Artery Atherosclerosis; Carotid Endarterctomy. In: Wilkins RH, Rengachary SS, editors. Neurosurgery. New York: McGraw-Hill; 1996. p. 2103-2115.

42. Goldstein LB. Extracranial carotid artery stenosis. Stroke 2003;34(11):2767-73.

43. Endovascular versus surgical treatment in patients with carotid stenosis in the Carotid and Vertebral Artery Transluminal Angioplasty Study (CAVATAS): a randomised trial. Lancet 2001;357(9270):1729-37.

44. Spence D, Eliasziw M. Endarterectomy or angioplasty for treatment of carotid stenosis? Lancet 2001;357(9270):1722-3.

45. Naylor AR, Bolia A, Abbott RJ, Pye IF, Smith J, Lennard N, et al. Randomized study of carotid angioplasty and stenting versus carotid endarterectomy: a stopped trial. J Vasc Surg 1998;28(2):326-34.

46. Yadav JS, Roubin GS, Iyer S, Vitek J, King P, Jordan WD, et al. Elective stenting of the extracranial carotid arteries. Circulation 1997;95(2):376-81.

47. Manninen HI, Rasanen HT, Vanninen RL, Vainio P, Hippelainen M, Kosma VM. Stent placement versus percutaneous transluminal angioplasty of human carotid arteries in cadavers in situ: distal embolization and findings at intravascular US, MR imaging and histopathologic analysis. Radiology 1999;212(2):483-92.

48. Kastrup A, Groschel K, Krapf H, Brehm BR, Dichgans J, Schulz JB. Early outcome of carotid angioplasty and stenting with and without cerebral protection devices: a systematic review of the literature. Stroke 2003;34(3):813-9.

49. Cremonesi A, Manetti R, Setacci F, Setacci C, Castriota F. Protected carotid stenting: clinical advantages and complications of embolic protection devices in 442 consecutive patients. Stroke 2003;34(8):1936-41.

50. Carotid revascularization using endarterectomy or stenting systems (CARESS): phase I clinical trial. J Endovasc Ther 2003;10(6):1021-30.

51. Theiss W, Hermanek P, Mathias K, Ahmadi R, Heuser L, Hoffmann FJ, et al. Pro-CAS: a prospective registry of carotid angioplasty and stenting. Stroke 2004;35(9):2134-9.

52. Yadav JS, Wholey MH, Kuntz RE, Fayad P, Katzen BT, Mishkel GJ, et al. Protected carotid-artery stenting versus endarterectomy in high-risk patients. N Engl J Med 2004;351(15):1493-501.

53. Endarterectomy vs. Angioplasty in Patients with Symptomatic Severe Carotid Stenosis (EVA-3S) Trial. Cerebrovasc Dis 2004;18(1):62-5.

54. Featherstone RL, Brown MM, Coward LJ. International carotid stenting study: protocol for a randomised clinical trial comparing carotid stenting with endarterectomy in symptomatic carotid artery stenosis. Cerebrovasc Dis 2004;18(1):69-74.

55. Hobson RW, 2nd. CREST (Carotid Revascularization Endarterectomy versus Stent Trial): background, design, and current status. Semin Vasc Surg 2000;13(2):139-43.

56. Hobson RW, 2nd, Howard VJ, Brott TG, Howard G, Roubin GS, Ferguson RD. Organizing the Carotid Revascularization Endarterectomy versus Stenting Trial (CREST): National Institutes of Health, Health Care Financing Administration, and industry funding. Curr Control Trials Cardiovasc Med 2001;2(4):160-164.

57. Higashida RT, Meyers PM, Phatouros CC, Connors JJ, 3rd, Barr JD, Sacks D. Reporting standards for carotid artery angioplasty and stent placement. Stroke 2004;35(5):e112-34.

58. Kalender WA, Seissler W, Klotz E, Vock P. Spiral volumetric CT with single-breath-hold technique, continuous transport, and continuous scanner rotation. Radiology 1990;176(1):181-3.

59. Crawford CR, King KF. Computed tomography scanning with simultaneous patient translation. Med Phys 1990;17(6):967-82.

60. Costello P, Ecker CP, Tello R, Hartnell GG. Assessment of the thoracic aorta by spiral CT. AJR Am J Roentgenol 1992;158(5):1127-30.

61. Napel S, Marks MP, Rubin GD, Dake MD, McDonnell CH, Song SM, et al. CT angiography with spiral CT and maximum intensity projection. Radiology 1992;185(2):607-10.

62. Schwartz RB, Jones KM, Chernoff DM, Mukherji SK, Khorasani R, Tice HM, et al. Common carotid artery bifurcation: evaluation with spiral CT. Work in progress. Radiology 1992;185(2):513-9.

63. Galanski M, Prokop M, Chavan A, Schaefer CM, Jandeleit K, Nischelsky JE. Renal arterial stenoses: spiral CT angiography. Radiology 1993;189(1):185-92.

64. Brink JA, Heiken JP, Balfe DM, Sagel SS, DiCroce J, Vannier MW. Spiral CT: decreased spatial resolution in vivo due to broadening of section-sensitivity profile. Radiology 1992;185(2):469-74.

65. Rubin GD, Dake MD, Napel SA, McDonnell CH, Jeffrey RB, Jr. Three-dimensional spiral CT angiography of the abdomen: initial clinical experience. Radiology 1993;186(1):147-52.

66. Stehling MK, Lawrence JA, Weintraub JL, Raptopoulos V. CT angiography: expanded clinical applications. AJR Am J Roentgenol 1994;163(4):947-55.

67. Sato Y, Shiraga N, Nakajima S, Tamura S, Kikinis R. Local maximum intensity projection (LMIP): a new rendering method for vascular visualization. J Comput Assist Tomogr 1998;22(6):912-7.

68. Kasales CJ, Hopper KD, Ariola DN, TenHave TR, Meilstrup JW, Mahraj RP, et al. Reconstructed helical CT scans: improvement in z-axis resolution compared with overlapped and nonoverlapped conventional CT scans. AJR Am J Roentgenol 1995;164(5):1281-4.

69. Polacin A, Kalender WA, Marchal G. Evaluation of section sensitivity profiles and image noise in spiral CT. Radiology 1992;185(1):29-35.

70. Rubin GD, Dake MD, Napel S, Jeffrey RB, Jr., McDonnell CH, Sommer FG, et al. Spiral CT of renal artery stenosis: comparison of three-dimensional rendering techniques. Radiology 1994;190(1):181-9.

71. Lawrence JA, Kim D, Kent KC, Stehling MK, Rosen MP, Raptopoulos V. Lower extremity spiral CT angiography versus catheter angiography. Radiology 1995;194(3):903-8.

72. Katz DA, Marks MP, Napel SA, Bracci PM, Roberts SL. Circle of Willis: evaluation with spiral CT angiography, MR angiography, and conventional angiography. Radiology 1995;195(2):445-9.

73. Stehling MK, Rosen MP, Weintraub J, Kim D, Raptopoulos V. Spiral CT venography of the lower extremity. AJR Am J Roentgenol 1994;163(2):451-3.

74. Casey SO, Alberico RA, Patel M, Jimenez JM, Ozsvath RR, Maguire WM, et al. Cerebral CT venography. Radiology 1996;198(1):163-70.

75. Remy-Jardin M, Remy J, Artaud D, Deschildre F, Duhamel A. Peripheral pulmonary arteries: optimization of the spiral CT acquisition protocol. Radiology 1997;204(1):157-63.

76. Johnson PT, Heath DG, Bliss DF, Cabral B, Fishman EK. Three-dimensional CT: real-time interactive volume rendering. AJR Am J Roentgenol 1996;167(3):581-3.

77. Berland LL, Smith JK. Multidetector-array CT: once again, technology creates new opportunities. Radiology 1998;209(2):327-9.

78. Rubin GD, Shiau MC, Schmidt AJ, Fleischmann D, Logan L, Leung AN, et al. Computed tomographic angiography: historical perspective and new state- of-the-art using multi detector-row helical computed tomography. J Comput Assist Tomogr 1999;23 Suppl 1:S83-90.

79. Thomsen HS, Morcos SK. In which patients should serum creatinine be measured before iodinated contrast medium administration? Eur Radiol 2005;15(4):749-54.

80. Tippins RB, Torres WE, Baumgartner BR, Baumgarten DA. Are screening serum creatinine levels necessary prior to outpatient CT examinations? Radiology 2000;216(2):481-4.

81. Brink JA, Lim JT, Wang G, Heiken JP, Deyoe LA, Vannier MW. Technical optimization of spiral CT for depiction of renal artery stenosis: in vitro analysis. Radiology 1995;194(1):157-63.

82. Wang G, Vannier MW. Maximum volume coverage in spiral computed tomography scanning. Acad Radiol 1996;3(5):423-8.

83. Brink JA, McFarland EG, Heiken JP. Helical/spiral computed body tomography. Clin Radiol 1997;52(7):489-503.

84. Rankin SC. CT angiography. Eur Radiol 1999;9(2):297-310.

85. Kalender WA, Prokop M. 3D CT angiography. Crit Rev Diagn Imaging 2001;42(1):1-28.

86. Rydberg J, Buckwalter KA, Caldemeyer KS, Phillips MD, Conces DJ, Jr., Aisen AM, et al. Multisection CT: scanning techniques and clinical applications. Radiographics 2000;20(6):1787-806.

87. Prokop M. Multislice CT angiography. Eur J Radiol 2000;36(2):86-96.

88. Prokop M. General principles of MDCT. Eur J Radiol 2003;45(Suppl 1):S4-10.

89. Horton KM, Fishman EK. 3D CT angiography of the celiac and superior mesenteric arteries with multidetector CT data sets: preliminary observations. Abdom Imaging 2000;25(5):523-5.

90. Catalano C, Laghi A, Fraioli F, Pediconi F, Napoli A, Danti M, et al. High-resolution CT angiography of the abdomen. Abdom Imaging 2002;27(5):479-87.

91. Schoepf UJ, Becker CR, Hofmann LK, Das M, Flohr T, Ohnesorge BM, et al. Multislice CT angiography. Eur Radiol 2003;13(8):1946-61.

92. Imhof H, Czerny C, Dirisamer A. Head and neck imaging with MDCT. Eur J Radiol 2003;45 Suppl 1:S23-31.

93. Foley WD, Karcaaltincaba M. Computed tomography angiography: principles and clinical applications. J Comput Assist Tomogr 2003;27 Suppl 1:S23-30.

94. Prokop M. Technical principles and future trends. 4th Bracoo Symposium on Multi-Detector CT 2003:1-9.

95. van Hoe L, Marchal G, Baert AL, Gryspeerdt S, Mertens L. Determination of scan delay time in spiral CT-angiography: utility of a test bolus injection. J Comput Assist Tomogr 1995;19(2):216-20.

96. Brink JA. Contrast optimization and scan timing for single and multidetector-row computed tomography. J Comput Assist Tomogr 2003;27 Suppl 1:S3-8.

97. Bae KT, Heiken JP, Brink JA. Aortic and hepatic contrast medium enhancement at CT. Part I. Prediction with a computer model. Radiology 1998;207(3):647-55.

98. Fleischmann D. Use of high concentration contrast media: principles and rationale-vascular district. Eur J Radiol 2003;45 Suppl 1:S88-93.

99. Fleischmann D, Rubin GD, Bankier AA, Hittmair K. Improved uniformity of aortic enhancement with customized contrast medium injection protocols at CT angiography. Radiology 2000;214(2):363-71.

100. Weidekamm C. Low kVp settings improve contrast enhancement and reduce radiation exposure in spiral CT of pulmonary emboli. In: Baert AL, editor. ECR 2002; 2002; Wien Austria: Springer; 2002. p. 149.

101. Kirchgeorg MA, Prokop M. Increasing spiral CT benefits with postprocessing applications. Eur J Radiol 1998;28(1):39-54.

102. Rubin GD. Techniques for performing multidetector-row computed tomographic angiography. Tech Vasc Interv Radiol 2001;4(1):2-14.

103. Van Ooijen PM, Ho KY, Dorgelo J, Oudkerk M. Coronary Artery Imaging with Multidetector CT: Visualization Issues. Radiographics 2003;7:7.

104. Prokop M, Shin HO, Schanz A, Schaefer-Prokop CM. Use of maximum intensity projections in CT angiography: a basic review. Radiographics 1997;17(2):433-51.

105. Napel S, Rubin GD, Jeffrey RB, Jr. STS-MIP: a new reconstruction technique for CT of the chest. J Comput Assist Tomogr 1993;17(5):832-8.

106. Brink JA. Technical aspects of helical (spiral) CT. Radiol Clin North Am 1995;33(5):825-41.

107. Calhoun PS, Kuszyk BS, Heath DG, Carley JC, Fishman EK. Three-dimensional volume rendering of spiral CT data: theory and method. Radiographics 1999;19(3):745-64.

108. Rubin GD, Beaulieu CF, Argiro V, Ringl H, Norbash AM, Feller JF, et al. Perspective volume rendering of CT and MR images: applications for endoscopic imaging. Radiology 1996;199(2):321-30.

109. Prokop M, Engelke C. Vascular System. In: Prokop M, Galanski M, editors. Spiral and Multislice Computed Tomography of the Body. Stuttgart New York: Thieme; 2003. p. 844-851.

110. Olbricht CJ, Paul K, Prokop M, Chavan A, Schaefer-Prokop CM, Jandeleit K, et al. Minimally invasive diagnosis of renal artery stenosis by spiral computed tomography angiography. Kidney Int 1995;48(4):1332-7.

111. Van Hoe L, Vandermeulen D, Gryspeerdt S, Mertens L, Baert AL, Suetens P, et al. Assessment of accuracy of renal artery stenosis grading in helical CT angiography using maximum intensity projections. Eur Radiol 1996;6(5):658-64.

112. Beregi JP, Elkohen M, Deklunder G, Artaud D, Coullet JM, Wattinne L. Helical CT angiography compared with arteriography in the detection of renal artery stenosis. AJR Am J Roentgenol 1996;167(2):495-501.

113. Kaatee R, Beek FJ, de Lange EE, van Leeuwen MS, Smits HF, van der Ven PJ, et al. Renal artery stenosis: detection and quantification with spiral CT angiography versus optimized digital subtraction angiography. Radiology 1997;205(1):121-7.

114. Kim TS, Chung JW, Park JH, Kim SH, Yeon KM, Han MC. Renal artery evaluation: comparison of spiral CT angiography to intra-arterial DSA. J Vasc Interv Radiol 1998;9(4):553-9.

115. Johnson PT, Halpern EJ, Kuszyk BS, Heath DG, Wechsler RJ, Nazarian LN, et al. Renal artery stenosis: CT angiography--comparison of real-time volume-rendering and maximum intensity projection algorithms. Radiology 1999;211(2):337-43.

116. Wittenberg G, Kenn W, Tschammler A, Sandstede J, Hahn D. Spiral CT angiography of renal arteries: comparison with angiography. Eur Radiol 1999;9(3):546-51.

117. Wilhelm K, Wilsmann-Theis D, Sommer T, Leutner C, Textor J, Schild H. [CT angiography hemodynamically relevant to renal artery stenosis. Evaluation of AXIAL, MPR, MIP and SSD reconstruction procedures under standard investigation conditions]. Rofo 2000;172(2):161-7.

118. Willmann JK, Wildermuth S, Pfammatter T, Roos JE, Seifert B, Hilfiker PR, et al. Aortoiliac and renal arteries: prospective intraindividual comparison of contrast-enhanced three-dimensional MR angiography and multi-detector row CT angiography. Radiology 2003;226(3):798-811.

119. Verschuyl EJ, Kaatee R, Beek FJ, Pasterkamp G, Bush WH, Beutler JJ, et al. Renal artery origins: location and distribution in the transverse plane at CT. Radiology 1997;203(1):71-5.

120. Beregi JP, Mauroy B, Willoteaux S, Mounier-Vehier C, Remy-Jardin M, Francke J. Anatomic variation in the origin of the main renal arteries: spiral CTA evaluation. Eur Radiol 1999;9(7):1330-4.

121. Rankin SC, Jan W, Koffman CG. Noninvasive imaging of living related kidney donors: evaluation with CT angiography and gadolinium-enhanced MR angiography. AJR Am J Roentgenol 2001;177(2):349-55.

122. Kawashima A, Sandler CM, Ernst RD, Tamm EP, Goldman SM, Fishman EK. CT evaluation of renovascular disease. Radiographics 2000;20(5):1321-40.

123. Moll R, Dinkel HP. Value of the CT angiography in the diagnosis of common carotid artery bifurcation disease: CT angiography versus digital subtraction angiography and color flow Doppler. Eur J Radiol 2001;39(3):155-62.

124. Willinsky RA, Taylor SM, TerBrugge K, Farb RI, Tomlinson G, Montanera W. Neurologic Complications of Cerebral Angiography: Prospective Analysis of 2,899 Procedures and Review of the Literature. Radiology 2003;227(2):522-528.

125. Schwartz RB. Helical (spiral) CT in neuroradiologic diagnosis. Radiol Clin North Am 1995;33(5):981-95.

126. Kuszyk BS, Fishman EK. Technical aspects of CT angiography. Semin Ultrasound CT MR 1998;19(5):383-93.

127. Dillon EH, van Leeuwen MS, Fernandez MA, Eikelboom BC, Mali WP. CT angiography: application to the evaluation of carotid artery stenosis. Radiology 1993;189(1):211-9.

128. Marks MP, Napel S, Jordan JE, Enzmann DR. Diagnosis of carotid artery disease: preliminary experience with maximum-intensity-projection spiral CT angiography. AJR Am J Roentgenol 1993;160(6):1267-71.

129. Cumming MJ, Morrow IM. Carotid artery stenosis: a prospective comparison of CT angiography and conventional angiography [see comments]. AJR Am J Roentgenol 1994;163(3):517-23.

130. Leclerc X, Godefroy O, Pruvo JP, Leys D. Computed tomographic angiography for the evaluation of carotid artery stenosis. Stroke 1995;26(9):1577-81.

131. Link J, Mueller-Huelsbeck S, Brossmann J, Grabener M, Stock U, Heller M. Prospective assessment of carotid bifurcation disease with spiral CT angiography in surface shaded display (SSD)-technique. Comput Med Imaging Graph 1995;19(6):451-6.

132. Tarjan Z, Pozzi Mucelli F, Frezza F, Pozzi Mucelli R. Three-dimensional reconstructions of carotid bifurcation from CT images: evaluation of different rendering methods. Eur Radiol 1996;6(3):326-33.

133. Papp Z, Patel M, Ashtari M, Takahashi M, Goldstein J, Maguire W, et al. Carotid artery stenosis: optimization of CT angiography with a combination of shaded surface display and source images. AJNR Am J Neuroradiol 1997;18(4):759-63.

134. Magarelli N, Scarabino T, Simeone AL, Florio F, Carriero A, Salvolini U, et al. Carotid stenosis: a comparison between MR and spiral CT angiography. Neuroradiology 1998;40(6):367-73.

135. Cinat M, Lane CT, Pham H, Lee A, Wilson SE, Gordon I. Helical CT angiography in the preoperative evaluation of carotid artery stenosis. J Vasc Surg 1998;28(2):290-300.

136. Leclerc X, Godefroy O, Lucas C, Benhaim JF, Michel TS, Leys D, et al. Internal carotid arterial stenosis: CT angiography with volume rendering. Radiology 1999;210(3):673-82.

137. Marcus CD, Ladam-Marcus VJ, Bigot JL, Clement C, Baehrel B, Menanteau BP. Carotid arterial stenosis: evaluation at CT angiography with the volume- rendering technique. Radiology 1999;211(3):775-80.

138. Sameshima T, Futami S, Morita Y, Yokogami K, Miyahara S, Sameshima Y, et al. Clinical usefulness of and problems with three-dimensional CT angiography for the evaluation of arteriosclerotic stenosis of the carotid artery: comparison with conventional angiography, MRA, and ultrasound sonography. Surg Neurol 1999;51(3):301-8.

139. Verhoek G, Costello P, Khoo EW, Wu R, Kat E, Fitridge RA. Carotid bifurcation CT angiography: assessment of interactive volume rendering. J Comput Assist Tomogr 1999;23(4):590-6.

140. Anderson GB, Ashforth R, Steinke DE, Ferdinandy R, Findlay JM. CT angiography for the detection and characterization of carotid artery bifurcation disease. Stroke 2000;31(9):2168-74.

141. Binaghi S, Maeder P, Uske A, Meuwly JY, Devuyst G, Meuli RA. Three-dimensional computed tomography angiography and magnetic resonance angiography of carotid bifurcation stenosis. Eur Neurol 2001;46(1):25-34.

142. Randoux B, Marro B, Koskas F, Duyme M, Sahel M, Zouaoui A, et al. Carotid artery stenosis: prospective comparison of CT, three-dimensional gadolinium-enhanced MR, and conventional angiography. Radiology 2001;220(1):179-85.

143. Alvarez-Linera J, Benito-Leon J, Escribano J, Campollo J, Gesto R. Prospective evaluation of carotid artery stenosis: elliptic centric contrast-enhanced MR angiography and spiral CT angiography compared with digital subtraction angiography. AJNR Am J Neuroradiol 2003;24(5):1012-9.

144. Lell M, Wildberger JE, Heuschmid M, Flohr T, Stierstorfer K, Fellner FA, et al. [CT-angiography of the carotid artery: First results with a novel 16-slice-spiral-CT scanner]. Rofo Fortschr Geb Rontgenstr Neuen Bildgeb Verfahr 2002;174(9):1165-9.

145. Zeman RK, Berman PM, Silverman PM, Davros WJ, Cooper C, Kladakis AO, et al. Diagnosis of aortic dissection: value of helical CT with multiplanar reformation and three-dimensional rendering. AJR Am J Roentgenol 1995;164(6):1375-80.

146. Quint LE, Francis IR, Williams DM, Bass JC, Shea MJ, Frayer DL, et al. Evaluation of thoracic aortic disease with the use of helical CT and multiplanar reconstructions: comparison with surgical findings. Radiology 1996;201(1):37-41.

147. Rieker O, Duber C, Neufang A, Pitton M, Schweden F, Thelen M. CT angiography versus intraarterial digital subtraction angiography for assessment of aortoiliac occlusive disease. AJR Am J Roentgenol 1997;169(4):1133-8.

148. Wicky S, Capasso P, Meuli R, Fischer A, von Segesser L, Schnyder P. Spiral CT aortography: an efficient technique for the diagnosis of traumatic aortic injury. Eur Radiol 1998;8(5):828-33.

149. Gomes MN, Davros WJ, Zeman RK. Preoperative assessment of abdominal aortic aneurysm: the value of helical and three-dimensional computed tomography. J Vasc Surg 1994;20(3):367-75.

150. Moritz JD, Rotermund S, Keating DP, Oestmann JW. Infrarenal abdominal aortic aneurysms: implications of CT evaluation of size and configuration for placement of endovascular aortic grafts. Radiology 1996;198(2):463-6.

151. Rubin GD, Paik DS, Johnston PC, Napel S. Measurement of the aorta and its branches with helical CT. Radiology 1998;206(3):823-9.

152. Lutz AM, Willmann JK, Pfammatter T, Lachat M, Wildermuth S, Marincek B, et al. Evaluation of aortoiliac aneurysm before endovascular repair: comparison of contrast-enhanced magnetic resonance angiography with multidetector row computed tomographic angiography with an automated analysis software tool. J Vasc Surg 2003;37(3):619-27.

153. Rofsky NM, Weinreb JC, Grossi EA, Galloway AC, Libes RB, Colvin SB, et al. Aortic aneurysm and dissection: normal MR imaging and CT findings after surgical repair with the continuous-suture graft-inclusion technique. Radiology 1993;186(1):195-201.

154. Sakai T, Dake MD, Semba CP, Yamada T, Arakawa A, Kee ST, et al. Descending thoracic aortic aneurysm: thoracic CT findings after endovascular stent-graft placement. Radiology 1999;212(1):169-74.

155. Armerding MD, Rubin GD, Beaulieu CF, Slonim SM, Olcott EW, Samuels SL, et al. Aortic aneurysmal disease: assessment of stent-graft treatment-CT versus conventional angiography. Radiology 2000;215(1):138-46.

156. Rubin GD, Shiau MC, Leung AN, Kee ST, Logan LJ, Sofilos MC. Aorta and iliac arteries: single versus multiple detector-row helical CT angiography. Radiology 2000;215(3):670-6.

157. Rubin GD, Schmidt AJ, Logan LJ, Sofilos MC. Multi-detector row CT angiography of lower extremity arterial inflow and runoff: initial experience. Radiology 2001;221(1):146-58.

158. Ota H, Takase K, Igarashi K, Chiba Y, Haga K, Saito H, et al. MDCT compared with digital subtraction angiography for assessment of lower extremity arterial occlusive disease: importance of reviewing cross-sectional images. AJR Am J Roentgenol 2004;182(1):201-9.

159. Amano Y, Ishihara M, Hayashi H, Gemma K, Kawamata H, Amano M, et al. Metallic artifacts of coronary and iliac arteries stents in MR angiography and contrast-enhanced CT. Clin Imaging 1999;23(2):85-9.

160. Ghaye B, Szapiro D, Mastora I, Delannoy V, Duhamel A, Remy J, et al. Peripheral pulmonary arteries: how far in the lung does multi-detector row spiral CT allow analysis? Radiology 2001;219(3):629-36.

161. Remy J, Remy-Jardin M, Wattinne L, Deffontaines C. Pulmonary arteriovenous malformations: evaluation with CT of the chest before and after treatment. Radiology 1992;182(3):809-16.

162. Hopkins KL, Patrick LE, Simoneaux SF, Bank ER, Parks WJ, Smith SS. Pediatric great vessel anomalies: initial clinical experience with spiral CT angiography. Radiology 1996;200(3):811-5.

163. Kim TH, Kim YM, Suh CH, Cho DJ, Park IS, Kim WH, et al. Helical CT angiography and three-dimensional reconstruction of total anomalous

pulmonary venous connections in neonates and infants. AJR Am J Roentgenol 2000;175(5):1381-6.

164. Velthuis BK, Rinkel GJ, Ramos LM, Witkamp TD, van der Sprenkel JW, Vandertop WP, et al. Subarachnoid hemorrhage: aneurysm detection and preoperative evaluation with CT angiography. Radiology 1998;208(2):423-30.

165. Kangasniemi M, Makela T, Koskinen S, Porras M, Poussa K, Hernesniemi J. Detection of intracranial aneurysms with two-dimensional and three-dimensional multislice helical computed tomographic angiography. Neurosurgery 2004;54(2):336-40.

166. Qanadli SD, El Hajjam M, Mesurolle B, Lavisse L, Jourdan O, Randoux B, et al. Motion artifacts of the aorta simulating aortic dissection on spiral CT. J Comput Assist Tomogr 1999;23(1):1-6.

167. Rubin GD, Leung AN, Robertson VJ, Stark P. Thoracic spiral CT: influence of subsecond gantry rotation on image quality. Radiology 1998;208(3):771-6.

168. Roos JE, Willmann JK, Weishaupt D, Lachat M, Marincek B, Hilfiker PR. Thoracic aorta: motion artifact reduction with retrospective and prospective electrocardiography-assisted multi-detector row CT. Radiology 2002;222(1):271-7.

169. Achenbach S, Giesler T, Ropers D, Ulzheimer S, Derlien H, Schulte C, et al. Detection of coronary artery stenoses by contrast-enhanced, retrospectively electrocardiographically-gated, multislice spiral computed tomography. Circulation 2001;103(21):2535-8.

170. Rodenwaldt J. Multislice computed tomography of the coronary arteries. Eur Radiol 2003;13(4):748-57.

171. Ropers D, Baum U, Pohle K, Anders K, Ulzheimer S, Ohnesorge B, et al. Detection of coronary artery stenoses with thin-slice multi-detector row spiral computed tomography and multiplanar reconstruction. Circulation 2003;107(5):664-6.

172. Nieman K, Cademartiri F, Lemos PA, Raaijmakers R, Pattynama PM, de Feyter PJ. Reliable noninvasive coronary angiography with fast submillimeter multislice spiral computed tomography. Circulation 2002;106(16):2051-4.

173. Stanford W, Thompson BH, Weiss RM. Coronary artery calcification: clinical significance and current methods of detection. AJR Am J Roentgenol 1993;161(6):1139-46.

174. Dean BL, Borden N. Imaging of carotid artery disease. Conventional angiography. Neuroimaging Clin N Am 1996;6(4):843-51.

175. Hunter JV, Chin JK. Carotid Angiography. In: Strandness DE, Breda Av, editors. Vascular Diseases. New York: Churchill Livingstone; 1994. p. 273-287.

176. Heiserman JE, Dean BL, Hodak JA, Flom RA, Bird CR, Drayer BP, et al. Neurologic complications of cerebral angiography. AJNR Am J Neuroradiol 1994;15(8):1401-7.

177. Bendszus M, Koltzenburg M, Burger R, Warmuth-Metz M, Hofmann E, Solymosi L. Silent embolism in diagnostic cerebral angiography and neurointerventional procedures: a prospective study. Lancet 1999;354(9190):1594-7.

178. Martin LG, Thiele BL. Diagnosis of Renovascular Disease. In: Strandess DE, Breda Av, editors. Vascular Diseases. New York: Chuchill Livingstone; 1994.

179. Klucznik RP. Current technology and clinical applications of three-dimensional angiography. Radiol Clin North Am 2002;40(4):711-28, v.

180. Kumazaki T. Development of rotational digital angiography and new cone-beam 3D image: clinical value in vascular lesions. Comput Methods Programs Biomed 1998;57(1-2):139-42.

181. Bosanac Z, Miller RJ, Jain M. Rotational digital subtraction carotid angiography: technique and comparison with static digital subtraction angiography. Clin Radiol 1998;53(9):682-7.

182. Elgersma OE, Buijs PC, Wust AF, van der Graaf Y, Eikelboom BC, Mali WP. Maximum internal carotid arterial stenosis: assessment with rotational angiography versus conventional intraarterial digital subtraction angiography. Radiology 1999;213(3):777-83.

183. Seymour HR, Matson MB, Belli AM, Morgan R, Kyriou J, Patel U. Rotational digital subtraction angiography of the renal arteries: technique and evaluation in the study of native and transplant renal arteries. Br J Radiol 2001;74(878):134-41.

184. Yuan C, Tsuruda JS, Beach KN, Hayes CE, Ferguson MS, Alpers CE, et al. Techniques for high-resolution MR imaging of atherosclerotic plaque. J Magn Reson Imaging 1994;4(1):43-9.

185. Toussaint JF, Southern JF, Fuster V, Kantor HL. T2-weighted contrast for NMR characterization of human atherosclerosis. Arterioscler Thromb Vasc Biol 1995;15(10):1533-42.

186. Toussaint JF, LaMuraglia GM, Southern JF, Fuster V, Kantor HL. Magnetic resonance images lipid, fibrous, calcified, hemorrhagic, and thrombotic components of human atherosclerosis in vivo. Circulation 1996;94(5):932-8.

187. Luo Y, Polissar N, Han C, Yarnykh V, Kerwin WS, Hatsukami TS, et al. Accuracy and uniqueness of three in vivo measurements of atherosclerotic carotid plaque morphology with black blood MRI. Magn Reson Med 2003;50(1):75-82.

188. Barkhausen J, Ebert W, Heyer C, Debatin JF, Weinmann HJ. Detection of atherosclerotic plaque with Gadofluorine-enhanced magnetic resonance imaging. Circulation 2003;108(5):605-9.

189. Hatsukami TS, Ross R, Polissar NL, Yuan C. Visualization of fibrous cap thickness and rupture in human atherosclerotic carotid plaque in vivo with high-resolution magnetic resonance imaging. Circulation 2000;102(9):959-64.

190. Yuan C, Mitsumori LM, Ferguson MS, Polissar NL, Echelard D, Ortiz G, et al. In vivo accuracy of multispectral magnetic resonance imaging for identifying lipid-rich necrotic cores and intraplaque hemorrhage in advanced human carotid plaques. Circulation 2001;104(17):2051-6.

191. Chu B, Kampschulte A, Ferguson MS, Kerwin WS, Yarnykh VL, O'Brien KD, et al. Hemorrhage in the atherosclerotic carotid plaque: a high-resolution MRI study. Stroke 2004;35(5):1079-84.

192. Kerwin W, Hooker A, Spilker M, Vicini P, Ferguson M, Hatsukami T, et al. Quantitative magnetic resonance imaging analysis of neovasculature volume in carotid atherosclerotic plaque. Circulation 2003;107(6):851-6.

193. Murphy RE, Moody AR, Morgan PS, Martel AL, Delay GS, Allder S, et al. Prevalence of complicated carotid atheroma as detected by magnetic resonance direct thrombus imaging in patients with suspected carotid artery stenosis and previous acute cerebral ischemia. Circulation 2003;107(24):3053-8.

194. Ruehm SG, Corot C, Vogt P, Kolb S, Debatin JF. Magnetic resonance imaging of atherosclerotic plaque with ultrasmall superparamagnetic particles of iron oxide in hyperlipidemic rabbits. Circulation 2001;103(3):415-22.

195. Flacke S, Fischer S, Scott MJ, Fuhrhop RJ, Allen JS, McLean M, et al. Novel MRI contrast agent for molecular imaging of fibrin: implications for detecting vulnerable plaques. Circulation 2001;104(11):1280-5.

196. Masaryk TJ, II JP, Dagirmanjian A, Tkach JA, Laub G. Magnetic Resonance Angiography: Neuroradiological Applications. In: Stark DD, Bradley WB, editors. Magnetic Resonance Imaging. St Louis: Mosby; 1999. p. 1277-1297.

197. Link KM, Lesko NM. Magnetic Resonance Angiography: Great Vessels and Abdomen. In: Stark DD, Bradley WG, editors. Magnetic resoance Imaging. St Louis: Mosby; 1999. p. 373-384.

198. De Marco JK, Nesbit GM, Wesbey GE, Richardson D. Prospective evaluation of extracranial carotid stenosis: MR angiography with maximum-intensity projections and multiplanar reformation compared with conventional angiography. AJR Am J Roentgenol 1994;163(5):1205-12.

199. Carriero A, Scarabino T, Magarelli N, Marano R, Ambrosini R, Salvolini U, et al. High-resolution magnetic resonance angiography of the internal carotid artery: 2D vs 3D TOF in stenotic disease. Eur Radiol 1998;8(8):1370-2.

200. Vanninen RL, Manninen HI, Partanen PL, Vainio PA, Soimakallio S. Carotid artery stenosis: clinical efficacy of MR phase-contrast flow quantification as an adjunct to MR angiography. Radiology 1995;194(2):459-67.

201. Serfaty JM, Chirossel P, Chevallier JM, Ecochard R, Froment JC, Douek PC. Accuracy of three-dimensional gadolinium-enhanced MR angiography in the assessment of extracranial carotid artery disease. AJR Am J Roentgenol 2000;175(2):455-63.

202. De Marco JK, Schonfeld S, Keller I, Bernstein MA. Contrast-enhanced carotid MR angiography with commercially available triggering mechanisms and elliptic centric phase encoding. AJR Am J Roentgenol 2001;176(1):221-7.

203. Herborn CU, Goyen M, Quick HH, Bosk S, Massing S, Kroeger K, et al. Whole-body 3D MR angiography of patients with peripheral arterial occlusive disease. AJR Am J Roentgenol 2004;182(6):1427-34.

204. Lee VS, Rusinek H, Noz ME, Lee P, Raghavan M, Kramer EL. Dynamic three-dimensional MR renography for the measurement of single kidney function: initial experience. Radiology 2003;227(1):289-94.

205. Remonda L, Senn P, Barth A, Arnold M, Lovblad KO, Schroth G. Contrast-enhanced 3D MR angiography of the carotid artery: comparison

with conventional digital subtraction angiography. AJNR Am J Neuroradiol 2002;23(2):213-9.

206. Derdeyn CP. Catheter angiography is still necessary for the measurement of carotid stenosis. AJNR Am J Neuroradiol 2003;24(9):1737-8.

207. Tunick PA, Krinsky GA, Lee VS, Kronzon I. Diagnostic imaging of thoracic aortic atherosclerosis. AJR Am J Roentgenol 2000;174(4):1119-25.

208. Zwiebel WJ. Ultrasound Assessment of Carotid Plaque. In: Zwiebel WJ, editor. Introduction to Vascular Ultrasonography. Philadelphia: W.B. Saunders Company; 2000. p. 125-135.

209. Biasi GM, Froio A, Diethrich EB, Deleo G, Galimberti S, Mingazzini P, et al. Carotid plaque echolucency increases the risk of stroke in carotid stenting: the Imaging in Carotid Angioplasty and Risk of Stroke (ICAROS) study. Circulation 2004;110(6):756-62.

210. AbuRahma AF, Wulu JT, Jr., Crotty B. Carotid plaque ultrasonic heterogeneity and severity of stenosis. Stroke 2002;33(7):1772-5.

211. Salonen RM, Nyyssonen K, Kaikkonen J, Porkkala-Sarataho E, Voutilainen S, Rissanen TH, et al. Six-year effect of combined vitamin C and E supplementation on atherosclerotic progression: the Antioxidant Supplementation in Atherosclerosis Prevention (ASAP) Study. Circulation 2003;107(7):947-53.

212. Zagzebski JA. Physics and Instrumantation in Doppler and B-mode Ultrasonography. In: Zwiebel WJ, editor. Introduction to Vascular Ultrasonography. Philadelphia: W.B. Saunders Company; 2000. p. 17-43.

213. Zwiebel WJ. Doppler Evaluation of Carotid Stenosis. In: Zwiebel WJ, editor. Introduction to Vascular Ultrasonography. Philadelphia: W.B. Sauders Company; 2000. p. 137-154.

214. Calliada F, Verga L, Pozza S, Bottinelli O, Campani R. Selection of patients for carotid endarterectomy: the role of ultrasound. J Comput Assist Tomogr 1999;23 Suppl 1:S75-81.

215. Eliasziw M, Rankin RN, Fox AJ, Haynes RB, Barnett HJ. Accuracy and prognostic consequences of ultrasonography in identifying severe carotid artery stenosis. North American Symptomatic Carotid Endarterectomy Trial (NASCET) Group. Stroke 1995;26(10):1747-52.

216. Howard G, Baker WH, Chambless LE, Howard VJ, Jones AM, Toole JF. An approach for the use of Doppler ultrasound as a screening tool for hemodynamically significant stenosis (despite heterogeneity of Doppler performance). A multicenter experience. Asymptomatic Carotid Atherosclerosis Study Investigators. Stroke 1996;27(11):1951-7.

217. Grant EG, Benson CB, Moneta GL, Alexandrov AV, Baker JD, Bluth EI, et al. Carotid artery stenosis: gray-scale and Doppler US diagnosis--Society of Radiologists in Ultrasound Consensus Conference. Radiology 2003;229(2):340-6.

218. Zwiebel WJ. Duplex Evaluation of Native Renal Vessels and Renal Allografts. In: Zwiebel WJ, editor. Introduction to Vascular Ultrasonography. Philadelphia: W.B. Saunders; 2000. p. 455-475.

219. Bom N, Li W, van der Steen AF, Lancee CT, Cespedes EI, Slager CJ, et al. New developments in intravascular ultrasound imaging. Eur J Ultrasound 1998;7(1):9-14.

220. Nissen SE, Yock P. Intravascular ultrasound: novel pathophysiological insights and current clinical applications. Circulation 2001;103(4):604-16.

221. Manninen HI, Rasanen H, Vanninen RL, Berg M, Hippelainen M, Saari T, et al. Human carotid arteries: correlation of intravascular US with angiographic and histopathologic findings. Radiology 1998;206(1):65-74.

222. Wilson EP, White RA. Intravascular ultrasound. Surg Clin North Am 1998;78(4):561-74.

223. Nally JV, Jr., Black HR. State-of-the-art review: captopril renography--pathophysiological considerations and clinical observations. Semin Nucl Med 1992;22(2):85-97.

224. Mann SJ, Pickering TG, Sos TA, Uzzo RG, Sarkar S, Friend K, et al. Captopril renography in the diagnosis of renal artery stenosis: accuracy and limitations. Am J Med 1991;90(1):30-40.

225. Vallabhajosula S, Fuster V. Atherosclerosis: imaging techniques and the evolving role of nuclear medicine. J Nucl Med 1997;38(11):1788-96.

226. Kolodgie FD, Petrov A, Virmani R, Narula N, Verjans JW, Weber DK, et al. Targeting of apoptotic macrophages and experimental atheroma with radiolabeled annexin V: a technique with potential for noninvasive imaging of vulnerable plaque. Circulation 2003;108(25):3134-9.

227. Tatsumi M, Cohade C, Nakamoto Y, Wahl RL, Knight LC, Strauss HW, et al. Fluorodeoxyglucose uptake in the aortic wall at PET/CT: possible finding for active atherosclerosis Non-oncologic applications of radiolabeled peptides in nuclear medicine Molecular imaging in nuclear cardiology. Radiology 2003;229(3):831-7.

228. Schaar JA, De Korte CL, Mastik F, Strijder C, Pasterkamp G, Boersma E, et al. Characterizing vulnerable plaque features with intravascular elastography. Circulation 2003;108(21):2636-41.

229. MacNeill BD, Lowe HC, Takano M, Fuster V, Jang IK. Intravascular modalities for detection of vulnerable plaque: current status. Arterioscler Thromb Vasc Biol 2003;23(8):1333-42.

230. Rothwell PM, Gibson RJ, Slattery J, Sellar RJ, Warlow CP. Equivalence of measurements of carotid stenosis. A comparison of three methods on 1001 angiograms. European Carotid Surgery Trialists' Collaborative Group. Stroke 1994;25(12):2435-9.

231. Fleiss J. Statistical Methods For Rates and Proportions. 2nd ed. New York: Wiley & Son; 1981.

232. Soulez G, Oliva VL, Turpin S, Lambert R, Nicolet V, Therasse E. Imaging of renovascular hypertension: respective values of renal scintigraphy, renal Doppler US, and MR angiography. Radiographics 2000;20(5):1355-68; discussion 1368-72.

233. Vasbinder GB, Nelemans PJ, Kessels AG, Kroon AA, de Leeuw PW, van Engelshoven JM. Diagnostic tests for renal artery stenosis in patients suspected of having renovascular hypertension: a meta-analysis. Ann Intern Med 2001;135(6):401-11.

234. Vasbinder GB, Nelemans PJ, Kessels AG, Kroon AA, Maki JH, Leiner T, et al. Accuracy of computed tomographic angiography and magnetic resonance angiography for diagnosing renal artery stenosis. Ann Intern Med 2004;141(9):674-82.

235. Schoenberg SO, Rieger J, Weber CH, Michaely HJ, Waggershauser T, Ittrich C, et al. High-Spatial-Resolution MR Angiography of Renal Arteries with Integrated Parallel Acquisitions: Comparison with Digital Subtraction Angiography and US. Radiology 2005;235(2):687-98.

236. Glagov S, Weisenberg E, Zarins CK, Stankunavicius R, Kolettis GJ. Compensatory enlargement of human atherosclerotic coronary arteries. N Engl J Med 1987;316(22):1371-5.

237. Liu Y, Hopper KD, Mauger DT, Addis KA. CT angiographic measurement of the carotid artery: optimizing visualization by manipulating window and level settings and contrast material attenuation. Radiology 2000;217(2):494-500.

238. Suzuki S, Furui S, Kaminaga T, Yamauchi T. Measurement of vascular diameter in vitro by automated software for CT angiography: effects of inner diameter, density of contrast medium, and convolution kernel. AJR Am J Roentgenol 2004;182(5):1313-7.

239. Wutke R, Lang W, Fellner C, Janka R, Denzel C, Lell M, et al. High-resolution, contrast-enhanced magnetic resonance angiography with elliptical centric k-space ordering of supra-aortic arteries compared with selective X-ray angiography. Stroke 2002;33(6):1522-9.

240. McCarthy MJ, Loftus IM, Thompson MM, Jones L, London NJ, Bell PR, et al. Angiogenesis and the atherosclerotic carotid plaque: an association between symptomatology and plaque morphology. J Vasc Surg 1999;30(2):261-8.

241. Chen CJ, Lee TH, Hsu HL, Tseng YC, Lin SK, Wang LJ, et al. Multi-Slice CT angiography in diagnosing total versus near occlusions of the internal

carotid artery: comparison with catheter angiography. Stroke 2004;35(1):83-5.

242. Villablanca JP, Jahan R, Hooshi P, Lim S, Duckwiler G, Patel A, et al. Detection and characterization of very small cerebral aneurysms by using 2D and 3D helical CT angiography. AJNR Am J Neuroradiol 2002;23(7):1187-98.

APPENDIX: Original articles

Kuopio University Publications D. Medical Sciences

D 339. Pellikainen, Johanna. Activator protein -2 in breast cancer: relation to cell growth, differentiation and cell-matrix interactions.
2004. 81 p. Acad. Diss.

D 340. Nunes, Sílvia Ramos. Longitudinal clinical characterization of the acute respiratory distress syndrome (ARDS): with special reference to monitoring of respiratory mechanics.
2004. 108 p. Acad. Diss.

D 341. Punakallio, Anne. Balance abilities of workers in physically demanding jobs: with special reference to firefighters of different ages.
2004. 87 p. Acad. Diss.

D 342. Lupsakko, Taina. Functional visual and hearing impairment in a population aged 75 years and older in the City of Kuopio in Finland: associations with mood and activities of daily living.
2004. 72 p. Acad. Diss.

D 343. Sivenius, Katariina. Genetic studies on type 2 diabetes mellitus with special emphasis on obesity and microvascular complications.
2004. 140 p. Acad. Diss.

D 344. Ylinen, Jari. Treatment of chronic non-specific neck pain with emphasis on strength training.
2004. 99 p. Acad. Diss.

D 345. Sironen, Reijo. Gene expression profiles of chondrocytic cells exposed to hydrostatic pressure.
2004. 77 p. Acad. Diss.

D 346. Lapveteläinen, Tuomo. Effects of aging, training, and collagen gene defects on murine osteoarthritis.
2004. 76 p. Acad. Diss.

D 347. Purhonen, Maija. Event-related potential (ERP) studies of mother-infant interaction.
2004. 90 p. Acad. Diss.

D 348. Inkinen, Ritva. Proteoglycans and hyaluronan in the intervertebral disc and cartilage endplate: effects of aging and degeneration.
2004. 97 p. Acad. Diss.

D 349. Salonvaara, Marjut. Coagulation physiology and abnormalities in newborn infants: association with intraventricular haemorrhage and central venous catheter-related thrombosis.
2004. 97 p. Acad. Diss.

D 350. Randell, Kaisa. Effects of hormonal and other factors on fractures in peri- and early postmenopausal women.
2004. 89 p. Acad. Diss.

D 351. Laasonen-Balk, Teijamari. Neuroimaging of depression using single-photon emission computerized tomography.
2005. 102 p. Acad. Diss.

D 352. Tolmunen, Tommi. Depression, B vitamins and homocysteine.
2005. 130 p. Acad. Diss.